Zebrafish as research model to study Gaucher disease: Insights into molecular mechanisms

Lelieveld, L.T.

CHAPTER 6

The detrimental role of excessive GlcSph during GCase deficiency in zebrafish

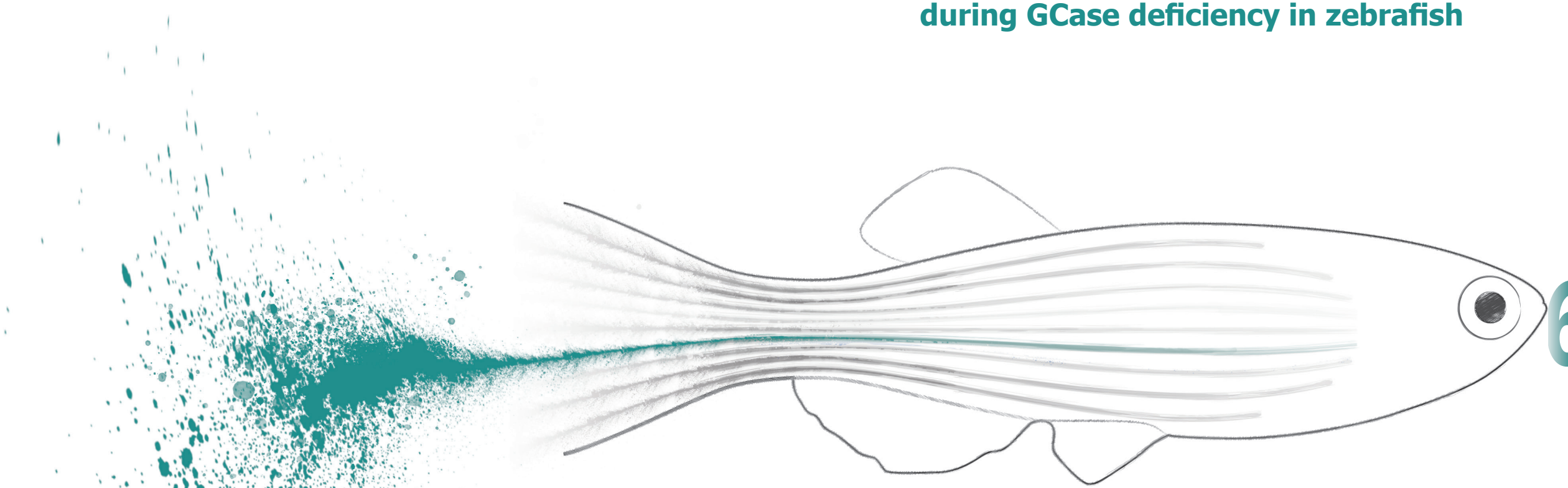

Manuscript in preparation:

Lelieveld LT, Gerhardt S, Maas S, Zwiers KC, de Wit KCC, Beijk EH, Ferraz MJ, Artola M, Meijer AH, Tudorache C, Salvatori D, Boot RG and Aerts JMFG

- The detrimental role of excessive glucosylsphingosine during glucocerebrosidase deficiency

Abstract

Deficiency of β-glucosidase (GCase) underlies Gaucher disease (GD), a lysosomal storage disorder. GD patients convert part of accumulating glucosylceramide through lysosomal acid ceramidase to the sphingoid base glucosylsphingosine (GlcSph). Chronically elevated GlcSph in blood and tissues of GD patients is thought to contribute to pathology. GCase-deficient *gba1* knockout (KO) zebrafish are viable and develop markedly increased GlcSph. Zebrafish have two orthologues of human acid ceramidase (ACase): Asah1a and Asah1b. From both single ACase KO fish only the *asah1b* KO fish fail to produce excessive GlcSph during GCase deficiency, while combined deficiency of both Asah1a and Asah1b is required to accumulate ceramide. Contrary to *gba1* KO fish, double deficient *gba1*:*asah1b* KO zebrafish show an ameliorated course of disease as reflected by a significant increase in lifespan (30-50%), with delayed development of abnormal locomotor activity and curved back. Both *gba1* and *gba1:asah1b* KO fish showed comparable GlcCer accumulation in tissues and similar induction in expression of storage-cell biomarkers chitinase (*chia.6*) and gpnmb. Infiltration of Gaucher-like cells in the periventricular grey zone of the optic tectum also appears comparable. In their brains the two mutant fish showed similar autophagy, indicated by increased protein levels of p62, and inflammation, reflected by increased mRNA levels of *il1-β*, *tnf*β and *apoeb*, as well as indications for similar activation of the complement cascade. In conclusion, the generated mutant zebrafish suggest that excessive GlcSph, generated *in vivo* by ACase, is detrimental. Abolishing Asah1b-ACase results in some phenotypic improvements but it does not prevent all abnormalities such as storage cell formation and neuroinflammation.

Introduction

Glucosylceramide (GlcCer) is a ubiquitous glycosphingolipid in cells and lipoproteins that acts as precursor of more complex glycosphingolipids. The breakdown of glycosphingolipids takes place in lysosomes where the penultimate step is catalysed by the acid β-glucosidase, named glucocerebrosidase (GCase) encoded by the *GBA* gene. Deficient activity of this enzyme causes Gaucher disease in which GlcCer characteristically accumulates in lysosomes of tissue macrophages that transform into storage cells. These 'Gaucher cells' are viable and secrete specific proteins into the circulation such as the enzyme chitotriosidase, the chemokine CCL18 and a soluble fragment of gpNMB[1-3]. The plasma levels of these proteins are clearly increased in symptomatic Gaucher patients and are presently used to assess the body burden of lipid-laden macrophages in patients[4-6]. More recently it has become clear that Gaucher cells are also the main source of the more than hundred-fold elevated glucosylsphingosine (GlcSph) in plasma of Gaucher patients[7]. This striking abnormality is widely employed to monitor Gaucher patients and assist diagnosis[7]. It has been speculated that excessive GlcSph contributes to signs and symptoms of Gaucher disease (see Ferraz *et al.* for a review[8]), including B cell activation and proliferation, aggregation of α-synuclein in Parkinson's disease, impairment of osteoblast and a harmful role on cerebral microvasculature[9-13]. Moreover, repeated intravenous administration of a relative high dose of GlcSph to mice induces formation of lipid laden storage cells resembling Gaucher cells as well as hepatosplenomegaly and haematological symptoms[14]. Although these findings suggest direct and concentration-dependent roles for GlcSph in the pathological manifestations of Gaucher disease, the translation of findings made with *in vitro* experiments are hampered by the current lack of knowledge of local (sub)cellular concentration of GlcSph during GCase deficiency. Furthermore, it should be taken into account that high concentrations of GlcSph act as inhibitor of GCase and therefore may reduce any catalytic activity of the enzyme[15]. Because of this, the harmful effects observed upon chronic administration of excessive amounts of GlcSph might be partly indirect[14].

Genetic and pharmacological evidence has been provided for the key role of acid ceramidase (ACase) in the excessive formation of GlcSph during GCase deficiency[16]. It was shown that fibroblasts from Farber patients, with inherited deficiency of ACase, do not form GlcSph upon inactivation of GCase as wildtype (WT) cells do. ACase (*N*-acylsphingosine deacylase; E.C. 3.5.1.23) is encoded by the gene (*ASAH1*) located on chromosome 8. ACase deficiency leads to the lysosomal storage disorder Farber disease (FD), with cells of classic FD patients typically showing less than 10% residual ACase activity. In spinal muscular atrophy with progressive myoclonic epilepsy (SMA-PME), ACase activity is also reduced but residual activity is higher, as much as 32% of controls[17,18]. Classic FD is characterized by deformed joints, subcutaneous nodules and progressive hoarseness, with neurological symptoms in severe patients. ACase hydrolyses ceramide (Cer) with a pH optimum of 4.5–5.0, rendering sphingosine and a free fatty acid as products. The enzyme is known to be able to catalyse the reverse reaction, generating Cer from sphingosine and free fatty acid at a pH optimum of 6.0 [19]. ACase is a heterodimer consisting of an α- (13 kDa) and a β-subunit (40 kDa)[20]. The enzyme is initially synthesized as N-glycated precursor and transported to lysosomes via mannose-6-phosphate mediated sorting. Inside the lysosome, ACase is

processed by autocleavage into the α and β subunits, thus freeing the catalytic cysteine residue at the novel N-terminus of the β-subunit and triggering a conformational change that opens up the active site for substrate entry[21-23].
The zebrafish has two orthologues of human ACase, Asah1a and Asah1b, and the latter enzyme has been studied best[24,25]. The consequences of Asah1b deficiency in zebrafish larvae have been investigated using morpholino knockdown[25]. Morphants showed degeneration of neurons in the spinal cord and less branched motor-neuron axons. The residual acid-ceramidase activity was about 26% and no increase in Cer levels was detected.

Zebrafish lacking lysosomal GCase have been generated using CRISPR/Cas9 technology[26]. The GCase-deficient fish are viable and rapidly develop increased levels of GlcSph, mimicking Gaucher disease[7]. Additionally, small compounds were developed that allow rapid, on-demand inactivation of GCase in zebrafish[27]. In this chapter, gene knockouts of *asah1a* and/or *asah1b* were generated and subsequently studied to evaluate if one or both enzymes are required for formation of GlcSph in zebrafish deficient in GCase. Interestingly, only Asah1b is involved in GlcSph formation during GCase deficiency. Raising the double deficient *gba1*$^{-/-}$*:asah1b*$^{-/-}$ fish, lacking excessive GlcSph, to adulthood revealed an improved phenotype compared to *gba1*$^{-/-}$ fish, with excessive GlcSph. Comparison of the mutant fish, at the predetermined end stage of 12 weeks post-fertilization (wpf), further indicated that the absence of GlcSph does not prevent inflammation in the brain nor impact on storage cells and increased GlcCer levels in liver and brain during GCase deficiency. The present study also uncovered that Asah1b deficiency alone does not cause severe accumulation of Cer. Active Asah1a seems to prevent this, given the observed Cer accumulation in *asah1a*$^{-/-}$*:asah1b*$^{-/-}$ zebrafish larvae. In conclusion, a unique Asah1b deficient zebrafish model is presented. Asah1b deficient zebrafish are unable to deacylate the accumulating primary GlcCer substrate in *gba1*$^{-/-}$*:asah1b*$^{-/-}$ and show an improved phenotype. In future endeavours, these Asah1b deficient zebrafish could enable the study of the impact of (toxic) lyso-lipids formed in other lysosomal storage disorders as well.

Figure 1| Alignment of the amino acid sequence of human ACase, zebrafish Asah1a and Asah1b ►
The amino acid sequences of the pre-mature human ACase (Uniprot code Q13510), zebrafish Asah1a (Uniprot code Q5XJR7) and Asah1b (Uniprot code Q6PH71) are aligned using ClustalO(1.2.4)[29]. * indicates a conserved residue between the three sequences, **:** a strongly similar residue and **.** a weakly similar residue. The signal peptide is predicted using SignalP-5.0 and depicted in blue[28]. Important residues in human ACase are coloured: the catalytic Cys143 is depicted in red, Cys31-Cys340 forming a disulfide bridge in pink, residues important for substrate hydrolysis and autocleavage in orange (Arg159 and Asp162, Glu225, Asn320 and Arg332) and the four assigned glycosylation sites in green[22].

Results

Two acid ceramidase orthologues in zebrafish: asah1a and asah1b

A protein BLAST with human acid ceramidase (UniProt accession Q13510) revealed two zebrafish co-orthologues: Asah1a (Uniprot accession Q5XJR7) and Asah1b (Uniprot accession Q6PH71). To investigate differences between the human protein and both zebrafish orthologs, the protein sequences of human ACase, Asah1a and Asah1b were aligned (**Figure 1**). The predicted Asah1a protein has 59% identity to the human protein, while Asah1b has 60% identity to the human ACase, albeit the proteins have 70% identity to each other. The predicted signal peptide showed the most variation (depicted in blue)[28]. The four potential N-glycosylation sites are present in both zebrafish Asah1 proteins (Asn 173, Asn 259, Asn 286 and Asn 342 in yellow)[22]. The catalytic cysteine (Cys 143) in human ACase, at the free N-terminus of the β-subunit after autocleavage, is present in a highly conserved region of both zebrafish Asah1 proteins (**Figure 1**). The α- and β-subunit of the mature heterodimeric human ACase protein are linked by a disulfide bond of Cys 31 and Cys 340, both being conserved in the zebrafish Asah1a and Asah1b proteins. Important residues in the β-subunit of human ACase, such as Arg 159, Asp 162, Glu 225 and Asn 320, are conserved in both zebrafish proteins (green and orange for Arg/Asp and Glu/Asn respectively). These amino acids are thought to play roles in stabilizing the catalytic N-terminus and/or positioning the ceramide substrate during hydrolysis [22].

```
                                          |30                                ↓1a-8
hACase      MPGRSCVALV-LLAAAVSCAVAQHAPPWTEDCRKSTYPPSGPTYRGAVPWYTINLDLPPY  59
Asah1a      ----MKLVFRYNALFISIFIHALYV-QGLEDCRSGMYPPKGPTYRGNVTWYTVNLDLPPS  55
Asah1b      MNNRLNLCFFI-LSYMCMCLSAQYVPPPFTEDCRSGMYPPNGPTFKGDVSWYTVDLDLPAS  59
                  : :             * :.    ****.. ***.***::* * ***::****
                                      ↓1b+11
hACase      KRWHELMLDKAPVLKVIVNSLKNMINTFVPSGKIMQVVDEKLPGLLGNFPGPFEEEMKGI  119
Asah1a      ERWTQIIKDKNTELIEMVQTIKDMAKGFF-HGKLVNFVDKELPFIVDTLPNPFNEEIKGI  114
Asah1b      KRWTDVISDKKTEMASMIQAIRDLADAFVPSGKLIQLVDKDLPLMVDTLPYPFNEEIRGI  119
            :** ::: **   :  :::::::: . *.  **:::.**:.** ::..:* **:**::**
                                     ▽          |160
hACase      AAVTDIPLGEIISFNIFYELFTICTSIVAEDKKGHLIHGRNMDFGVFLGWNINNDTWVIT  179
Asah1a      AAVSGIPLGEIALFNIFYEVFTVCTSLVAEDNNGNIYHGRNLDFGLFMGWDRQNKTWTLT  175
Asah1b      ASVSGVPLGEVVLFNIFYEVFTVCTSLVAEDVNGNLIHARNLDFGLFMGWDLKNRSWVIT  179
            *:*:.:****:  ******:**:***:**** :*:: *.**:***:*:**: :* :*.:*
                        |200                 |220
hACase      EQLKPLTVNLDFQRNNKTVFKASSFAGYVGMLTGFKPGLFSLTLNERFSINGGYLGILEW  239
Asah1a      EKLKPLVVNINFERKNQTVFKSTSFAGYVGMLTGIRPGELTLTMNERFDFDGGYIGILDW  235
Asah1b      EKLKPLVVNIDFTRNGQTVFKSTNFAGYVGMLTGIHQNSFTLTMNERFSLDGGYIGILEW  239
            *:****.**::* *:.:****::.**********:: . ::**:****.::***:***:*
                        |260                 |280
hACase      ILGKKDVMWIGFLTRTVLENSTSYEEAKNLLTKTKILAPAYFILGGNQSGEGCVITRDRK  299
Asah1a      IFGNRDGMWTGFLTRRVLENSTSYEDAKDQLSQTKLLAPVYFILGGNRTGQGCVITRTRI  294
Asha1b      ILGKRDGMWMSFLTRSVLENATSYESAKALLSDTKLLAPAYFILGGNQSGEACIITRSRT  299
            *:*::* ** .**** ****:****.**  *:.**:***.*******::*:.*:*** *
                        |320                 |340
hACase      ESLDVYELDAKQGRWYVVQTNYDRWKHPFFLDDRRTPAKMCLNRTSQENISFETMYDVLS  359
Asah1a      NTLDIWELELMLGRWYVLETNYDHWDKPMFLDDRRTPAMKCMNQTTQANISLASIYNVLS  355
Asah1b      QNISPLELNVKNGRWYVLETNYDHWKEPLFLDDRRTPAMKCMNQTTQTNISVKTVYDVLS  359
            :.:.  **:   *****::****:*..*:********* *:*:*:* ***. ::*:***
                        |380
hACase      TKPVLNKLTVYTTLIDVTKGQFETYLRDCPDPCIGW                        395
Asah1a      TKPVLNKLTTYTSLMAVSTGTLESYVRDCPNPCTPW                        390
Asah1b      TKPVLNKLTTYTTLMEVSKGTLESFIRDCPNPCMPW                        395
            *********.**:*: *:.* :*:::****:**  *
```

Generation of CRISPR/Cas9 mediated knockouts of Asah1a and Asah1b

To study the role of zebrafish ACases *in vivo*, CRISPR/Cas9 mediated knockouts of Asah1a and Asah1b were generated. SgRNA sequences were selected in the third exon of *asah1a*, located on chromosome 14, and the fourth exon of *asah1b* located on chromosome 1 (**Figure 2A** and **B**, top and middle panels). Injection of Cas9 mRNA and the appropriate sgRNA in the single-cell stage of wildtype (WT) embryos resulted in founder fish with a germline transmitted deletion of 8 bp for *asah1a* and an insertion of 11 bp for *asah1b* (**Figure 2A** and **B**, lower panels). The predicted stop-codons of these mutations are located in exon 3 and exon 4 for *asah1a* and *asah1b* respectively, both in the translated α-subunit (mutation marked in Figure 1 with an arrow), resulting in no functional β-subunit.

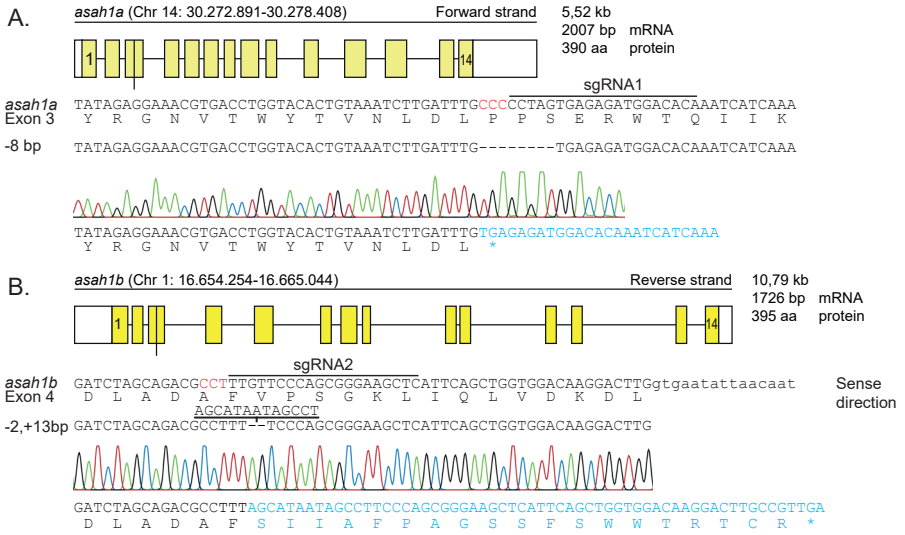

Figure 2| CRISPR/Cas9 mediated disruption of Asah1a and Asah1b in zebrafish

(A) Top panel: Schematic representation of the *asah1a* gene on chromosome 14, encoding the predicted 390 amino acid Asah1a enzyme. Middle panel: DNA sequence of exon 3 of *asah1a* with sgRNA target 1 lined, the PAM site in red and the protein sequence shown below. Lower panel: The 8 base pair deletion, as obtained from the sequence trace, leads to a premature stopcodon (*). **(B)** Top panel: Schematic representation of the *asah1b* gene on chromosome 4, encoding the predicted 395 amino acid Asah1b enzyme, with the exon in upper case and intron in lower case. Middle panel: DNA sequence of exon 4 of *asah1b* with sgRNA target 2 lined, the PAM site in red and the protein sequence shown below. Lower panel: The sequence trace showed an insertion of 11 base pairs, which leads to a change amino acid sequence and a premature stopcodon (*).

Only the double knockout of *asah1a:asah1b* accumulates primary substrate ceramide

Double heterozygous *asah1a*$^{+/-}$*:asah1b*$^{+/-}$ were crossed and lipid analysis of WT, *asah1a*$^{-/-}$, *asah1b*$^{-/-}$ and *asah1a*$^{-/-}$*:asah1b*$^{-/-}$ zebrafish larvae (5 dpf) showed that ceramide was only significantly increased in *asah1a*$^{-/-}$*:asah1b*$^{-/-}$ fish (**Figure 3A**). This finding indicates that Asah1a and Asah1b enzymes are both able to hydrolyse ceramide and that a single enzyme deficiency is not enough to cause ceramide accumulation.

Only Asah1b generates GlcSph during GCase deficiency

To study the role of either ACase in GCase deficiency we exposed developing zebrafish embryos lacking either Asah1a, Asah1b, or both, to a specific suicide inhibitor of GCase (ME656), known to rapidly inactivate the GCase enzyme[27]. Inhibitor treated WT zebrafish larvae (5 dpf) showed a significant increase in hexosylceramide (HexCer), primarily GlcCer as determined before[26], GlcChol and GlcSph (**Figure 3B** and **C**). Contrary to Asah1a-deficient larvae, the inhibitor-treated animals deficient in Asah1b did not show the striking GlcSph elevation, although Asah1b-deficient larvae did accumulate GlcChol and HexCer (**Figure 3C**). In addition, GlcSph levels did not increase in double genetic *gba1*$^{-/-}$*:asah1b*$^{-/-}$ larvae (**Supplementary Figure 1**). Thus, Asah1b in the zebrafish seems responsible for the generation of GlcSph during GCase deficiency.

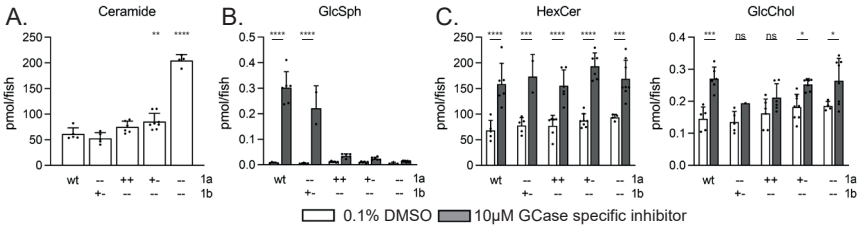

Figure 3 | (Glyco)sphingolipid abnormalities in Asah1a and/or Asah1b deficient zebrafish larvae

(A) Total ceramide levels were determined of individual zebrafish larvae (5 dpf) of off-spring of *Asah1a*$^{+/-}$*:asah1b*$^{+/-}$ crossings in pmol/fish. Data is depicted as mean ± SD and analysed using a Two-Way Anova with Tukey's multiple comparisons Test. **(B)** *Asah1a*$^{+/-}$*:asah1b*$^{+/-}$ adult zebrafish were crossed and off-spring was treated with vehicle (0.1% (v/v) DMSO) or 10 µm GCase specific inhibitor (ME656) for 5 days. Relevant lipid levels were determined of individual larvae in pmol/fish. WT (n = 5-6), *asah1a*$^{-/-}$*:asah1b*$^{+/-}$ (n = 1-5), *asah1*$^{+/+}$*:asah1b*$^{-/-}$ (n = 6), *asah1*$^{+/-}$*:asah1b*$^{-/-}$ (n = 7-8) and *asah1a*$^{-/-}$*:asah1b*$^{-/-}$ (n = 4-8). Data is depicted as mean ± SD and analysed using a Two-Way Anova with Sidak's multiple comparisons test. In general, statistical comparisons are depicted only when a significant difference is apparent and relevant. Ns = not significant, * P < 0.05,** P < 0.01, *** P < 0.001 and **** P < 0.0001.

Biochemical hallmarks in livers and brains of *gba1*$^{-/-}$ and *gba1*$^{-/-}$*:asah1b*$^{-/-}$ fish

WT, *gba1*$^{-/-}$ fish, *asah1b*$^{-/-}$ and double deficient *gba1*$^{-/-}$*:asah1b*$^{-/-}$ fish were raised to adulthood and (glyco)sphingolipid composition, mRNA expression, protein expression and histopathology of relevant organs were analysed at 12 weeks post-fertilization (wpf).
Gba1$^{-/-}$ adult zebrafish showed a phenotype as described before[30] and were culled at earlier stages when predetermined end points were observed (t = 10-11 wpf).

Gaucher-like cells in visceral organs of *gba1*$^{-/-}$*:asah1b*$^{-/-}$ fish

Excessive GlcSph was only detected in the livers of *gba1*$^{-/-}$ zebrafish (**Figure 4A**). GlcCer was increased comparably in gba*1*$^{-/-}$ and *gba1*$^{-/-}$*:asah1b*$^{-/-}$ livers (5000 pmol/mg, **Figure 4A**). GlcChol was significantly increased in *gba1*$^{-/-}$ fish (10 pmol/mg liver), but not in *gba1*$^{-/-}$*:asah1b*$^{-/-}$ fish. The livers of *gba1*$^{-/-}$*:asah1b*$^{-/-}$ fish showed minor increases of Cer, GalCer and LacCer (**Figure 4A**). This was not prominent in the tissues of *gba1*$^{-/-}$ fish and *asah1b*$^{-/-}$ fish.

Next, the expression of mRNAs encoding specific proteins were studied in livers of the different zebrafish (**Figure 4B**). A significant increase in expression of the storage-cell biomarker *gpnmb* was apparent in *gba1*$^{-/-}$ and *gba1*$^{-/-}$*:asah1b*$^{-/-}$ zebrafish livers. However, no prominent difference in expression of an orthologue of human chitotriosidase (*chia.6*) was detected, while the lysosomal protease Cathepsin D (*catD*) and the inflammatory cytokine *il-1*β showed a slight, but not significant increase and tnfβ showed only a significant increase in *gba1*$^{-/-}$ livers. To analyse the pathology of multiple different organs and tissues, the whole body of the fish was sectioned sagitally (**Figure 4C-E**).

The liver of zebrafish differs from the mammalian one: the zebrafish liver is not organized in hepatic lobules and Kupffer cells seem absent[31]. In addition, pancreatic cells of the zebrafish are scattered along the intestinal tract[31]. Infiltration of Gaucher-like cells was detected in the liver, spleen and pancreatic cell rich tissue of *gba1*$^{-/-}$ and *gba1*$^{-/-}$*:asah1b*$^{-/-}$ zebrafish (**Figure 4D** and **E**). Lesions with Gaucher-like cells were apparent in *gba1*$^{-/-}$*:asah1b*$^{-/-}$ tissue. No apparent pathological observations were noticed in tissues of *asah1b*$^{-/-}$ fish **(Supplementary Figure 2**).

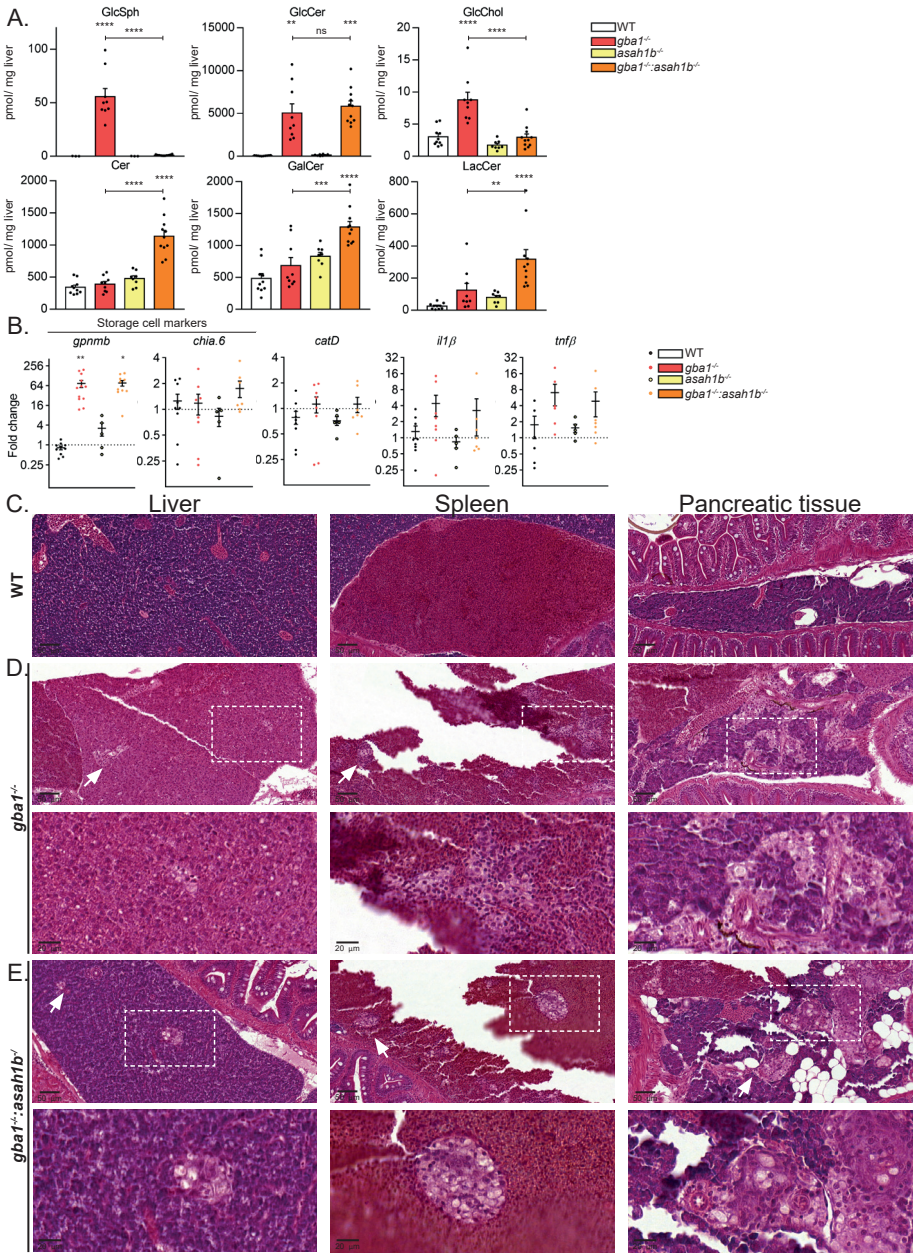

Figure 4 | Abnormalities in adult zebrafish visceral organs

(A) Lipid levels were determined in pmol/mg liver tissue. Data is depicted as mean ± SEM; WT (n = 10), *gba1*$^{-/-}$ (n = 9), *asah1b*$^{-/-}$ (n = 8), *gba1*$^{-/-}$*:asah1b*$^{-/-}$ (n = 11). Data is analysed by One-Way Anova (Dunnet's test) with WT as control group. **(B)** Expression of *gpnmb*, *chia.6*, *il-1*β, *tnf*β, *apoEb* or *catD* mRNA levels were determined using RT-qPCR analysis; WT (n = 6-9), *gba1*$^{-/-}$ (n = 6-8), *asah1b*$^{-/-}$ (n = 5), *gba1*$^{-/-}$*:asah1b*$^{-/-}$ (n = 7). Data is normalized using two housekeeping genes (*ef1α* and *rpl13*) and analysed by One-Way Anova (Dunnett's test) with WT as control group. H&E staining of liver, spleen and pancreatic tissue of WT **(C)**, gba1$^{-/-}$ **(D)** and *gba1*$^{-/-}$*:asah1b*$^{-/-}$ **(E)** zebrafish. Higher magnifications of oxed areas are shown below the respective lower magnifications. Ns = not significant, * P < 0.05,** P < 0.01, and **** P < 0.0001.

Similar lipid abnormalities, autophagy and inflammation in the brain of *gba1*$^{-/-}$*:asah1b*$^{-/-}$

Analysis of the lipid composition of brains of the mutant zebrafish and that of matched WT animals (**Figure 5A**) showed that the total Cer levels are normal. Accumulation of GlcSph is profound in brains of *gba1*$^{-/-}$ zebrafish (± 0.16 to 130 pmol/mg for brains of WT and *gba1*$^{-/-}$ respectively), while no significant increase in GlcSph levels is detected in brains of *gba1*$^{-/-}$*:asah1b*$^{-/-}$ zebrafish (± 10 pmol/mg). The primary substrate of GCase, GlcCer, is comparably elevated in brains of both *gba1*$^{-/-}$ and *gba1*$^{-/-}$*:asah1b*$^{-/-}$ (± 100-fold and 120-fold), as well as that of the product glycosphingolipid LacCer (± 22-fold and 33-fold, respectively). GlcChol is elevated in brains of gba1$^{-/-}$ zebrafish (± 2.5-fold) and slightly in brains of *gba1*$^{-/-}$*:asah1b*$^{-/-}$ fish (± 1.3-fold). The abundant myelin lipid GalCer is only slightly decreased in *gba1*$^{-/-}$ brains, however variation among individual fish in this lipid was marked.

Next, the expression of mRNAs in brains of the different zebrafish were analysed (**Figure 5B**). In both *gba1*$^{-/-}$ and *gba1*$^{-/-}$*:asah1b*$^{-/-}$ brains, expression of *gpnmb* and *chia.6* was strikingly increased (± 70-fold for *gpnmb* and c*hia.6*). In parallel, we observed increased expression of mRNAs of inflammatory cytokines *il1-β* (± 6.5-fold and 8.5-fold for brains *of gba1*$^{-/-}$ and *gba1*$^{-/-}$*:asah1b*$^{-/-}$ fish, respectively) and *tnf*β (± 17-fold and 30-fold) (**Figure 5B**). In addition, increased mRNA expression was noted in the brains of both *gba1*$^{-/-}$ and *gba1*$^{-/-}$*:asah1b*$^{-/-}$ for *catD* (2.5-3-fold), and the microglia marker *apoEb* (5-6-fold)[32,33]. Expression of several genes encoding components of the complement system (*c1qA*, *c3.1*, *c5* and the c5a receptor (*c5aR1*)) are significantly increased in both *gba1*$^{-/-}$ and *gba1*$^{-/-}$*:asah1b*$^{-/-}$ brains. Western blot analysis revealed that the amount of p62 and the ratio of LC3-II to LC3-I were increased in the brains of both *gba1*$^{-/-}$ and *gba1*$^{-/-}$*:asah1b*$^{-/-}$ zebrafish, indicating that autophagy was upregulated (**Figure 5C** and **D**).

H&E staining showed infiltration of Gaucher-like cells in brains of both *gba1*$^{-/-}$ and *gba1*$^{-/-}$*:asah1b*$^{-/-}$ fish, mainly in the periventricular grey zone of the optic tectum (**Figure 5E** with zoom in **Figure 5F**). These abnormal cells were not present in WT or *asah1b*$^{-/-}$ zebrafish brain (**Figure 5E** and **F** for WT, **Supplementary Figure 3** for *asah1b*$^{-/-}$). Transverse sections of the dienchephalon, showed infiltration of Gaucher-like cells in both brain halves (**Figure 5G**).

Figure 5 | Biochemical abnormalities in adult zebrafish brain ►

(A) Lipid levels were determined of dissected brains in pmol/mg tissue. Data is depicted as mean ± SEM; WT (n = 9-10), *gba1*$^{-/-}$ (n = 9), *asah1b*$^{-/-}$ (n = 8), *gba1*$^{-/-}$*:asah1b*$^{-/-}$ (n = 11). Data is analysed by Two-Way Anova with Dunnett's multiple comparison test and WT as control group. **(B)** mRNA levels of *asah1a, asah1b, gpnmb*, *chia.6*, *il-1*β, *tnf*β, *apoEb, catD, c1qA, c3.1, c5aR* and *c5* was determined using RT-qPCR analysis; WT (n = 9-11), *gba1*$^{-/-}$ (n = 8-11), *asah1b*$^{-/-}$ (n = 5), *gba1*$^{-/-}$*:asah1b*$^{-/-}$ (n = 9-10). **(C)** Representative western blot of p62, LC3-I, LC3-II, β-catenin protein levels in WT, *gba1*$^{-/-}$*, asah1b*$^{-/-}$ and *gba1*$^{-/-}$*:asah1b*$^{-/-}$ zebrafish brains, with β-actin as protein loading control. **(D)** Quantitative analysis of LC3-II/LC-I levels and p62 protein levels. WT (n = 5), *gba1*$^{-/-}$ (n = 5), *asah1b*$^{-/-}$ (n = 3), *gba1*$^{-/-}$*:asah1b*$^{-/-}$ (n = 6). **(E)** H&E staining of brain sagittal sections of WT, *gba1*$^{-/-}$ and *gba1*$^{-/-}$*:asah1b*$^{-/-}$, with infiltration of Gaucher-like in the periventricular grey zone of the optic tectum **(F)** in *gba1*$^{-/-}$ and *gba1*$^{-/-}$*:asah1b*$^{-/-}$ brains. **(G)** Transversal sectioning with storage cell infiltration in both halves of the periventricular grey zone of the optic tectum. **(H)** mRNA expression of *th1, th2, snc*β, *sncγa, sncγb* and *mbpa* was determined using RT-qPCR analysis; WT (n = 7), *gba1*$^{-/-}$ (n = 9), *asah1b*$^{-/-}$ (n = 4), *gba1*$^{-/-}$*:asah1b*$^{-/-}$ (n = 7). Data of RT-qPCR is normalized using two housekeeping genes (*ef1α* and *rpl13*), analysed by One-Way Anova with Tukey's multiple comparisons test or Brown-Forsythe and Welch Anova with Dunnett's multiple comparisons test for *gpnmb* and *chia.6* and depicted as scattered dot plot ± SEM. In general, statistical comparisons are depicted as WT vs *gba1*$^{-/-}$, WT vs *gba1*$^{-/-}$*:asah1b*$^{-/-}$ or *gba1*$^{-/-}$ vs *gba1*$^{-/-}$*:asah1b*$^{-/-}$, only when a significant difference is apparent and relevant. Ns = not significant, ** P < 0.01, *** P < 0.001 and **** P < 0.0001.

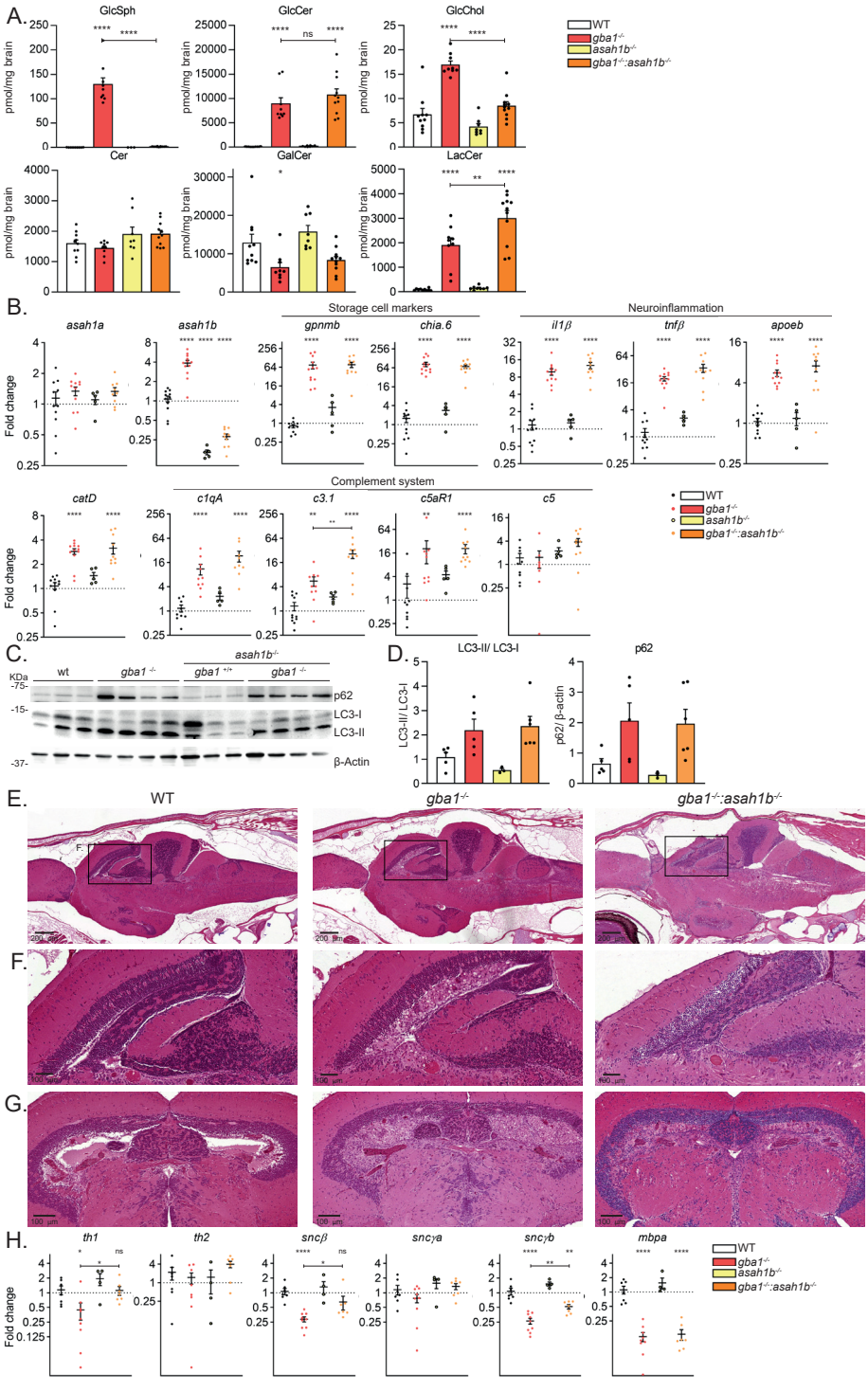
A.
GlcSph
GlcCer
GlcChol
Cer
GalCer
LacCer
pmol/mg brain
WT
gba1-/-
asah1b-/-
gba1-/-:asah1b-/-
B.
Storage cell markers
Neuroinflammation
Complement system
asah1a
asah1b
gpnmb
chia.6
il1β
tnfβ
apoeb
catD
c1qA
c3.1
c5aR1
c5
Fold change
C.
asah1b-/-
KDa
wt
gba1 -/-
gba1 +/+
gba1 -/-
p62
LC3-I
LC3-II
β-Actin
D.
LC3-II/ LC3-I
p62
p62/ β-actin
E.
WT
gba1-/-
gba1-/-:asah1b-/-
F.
G.
H.
th1
th2
sncβ
sncγa
sncγb
mbpa

Neurodegeneration was studied by analysis of mRNA levels of the two tyrosine hydroxylase orthologues in the zebrafish brains. A significant decrease in *th1*, but not *th2*, was observed in *gba1*$^{-/-}$ zebrafish brains, while no significant reduction was observed in the *gba1*$^{-/-}$*:asah1b*$^{-/-}$ brains (**Figure 5H**). In addition, two transcripts of zebrafish orthologues of α-synuclein, *snc*β and *snc*γ*b*, were significantly reduced in gba1$^{-/-}$ brains compared to WT and *gba1*$^{-/-}$*:asah1b*$^{-/-}$ brains. The expression of myelin-basic protein (*mbpa*) was comparably reduced in both *gba1*$^{-/-}$ and *gba1*$^{-/-}$*:asah1b*$^{-/-}$ brains. These mRNA findings could point to aberrant myelination in both mutants, while dopamine neurons appear to be only abnormal in *gba1*$^{-/-}$ fish at this age.

Phenotypic improvements of adult Asah1b:Gba1 double knockout zebrafish

In general, experiments were ended at 12 wpf, or earlier for individual *gba1*$^{-/-}$ zebrafish when predetermined human end points were observed (t = 10-12 wpf). Up to 8 wpf, no overt phenotype was observed in the WT, *gba1*$^{-/-}$, *asah1b*$^{-/-}$ and *gba1*$^{-/-}$*:asah1b*$^{-/-}$ fish. From 8 wpf onwards, a drop in the tail of individual *gba1*$^{-/-}$ zebrafish was apparent which progressively worsened from 9 to 12 wpf. Differences were noticeable among the different types of mutant fish as well as variation among individual fish within each genotype. All *gba1*$^{-/-}$ zebrafish (t= 10-12 wpf) showed phenotypic characteristics such as a curved back and different swimming behaviour (**Figure 7A**). The size of the *gba1*$^{-/-}$ zebrafish was significant smaller than WT, while the tortuosity, i.e. the length of the curved back divided by the length from head to tail base, was significantly enlarged (**Figure 7B**). Most of the *gba1*$^{-/-}$ fish showed abnormal swimming behaviour, ranging from difficulty with balance, failure to maintain an upright position to the inability to move from the bottom of the tank. Individual zebrafish were tracked to quantify their swimming speed and time spend in the upper part of the tank (**Figure 7C** and **D**). It was observed that tracking various *gba1*$^{-/-}$ fish was more difficult, as they did not move from the bottom of the tank. However, on average, *gba1*$^{-/-}$ zebrafish did not show bradykinesia, because the mean speed was not significantly different from WT (**Figure 7D**). A significant difference was observed in the ability of the zebrafish to use the whole tank. In contrast to WT fish, *gba1*$^{-/-}$ zebrafish spend significantly less time in the top of the tank (**Figure 7C** and **D**). These findings suggested that the *gba1*$^{-/-}$ zebrafish had abnormal swimming behaviour, predominantly manifested as the inability to use the entire tank, however on average they reach similar velocities as WT.

Contrary to *gba1*$^{-/-}$ fish, all *gba1*$^{-/-}$*:asah1b*$^{-/-}$ fish at 12 wpf showed no significant difference in length or tortuosity (**Figure 7A** and **B**). Additionally, *gba1*$^{-/-}$*:asah1b*$^{-/-}$ did not show postural imbalance and used the whole tank for swimming as the WT and *asah1b*$^{-/-}$ zebrafish (**Figure 7C** and **D**). Therefore, a pilot longevity study was performed by raising the *gba1*$^{-/-}$*:asah1b*$^{-/-}$ zebrafish past 12 wpf until similar phenotypic characteristics were apparent for the g*ba1*$^{-/-}$ zebrafish at 10 to 12 wpf. Individual double mutant zebrafish showed a curved back (**Figure 7E**), postural imbalance and abnormal swimming behaviour and therefore had to be culled around 15-17 wpf (**Figure 7F** and **Supplementary Figure 4**).

Thus, there was a marked amelioration of disease course by at least 5 weeks (33%) in the *gba1*$^{-/-}$*:asah1b*$^{-/-}$ zebrafish lacking excessive GlcSph. Importantly, the absence of GlcSph did not prevent, on the longer run, the development of phenotypic abnormalities such as the curved back and differences in swimming behaviour.

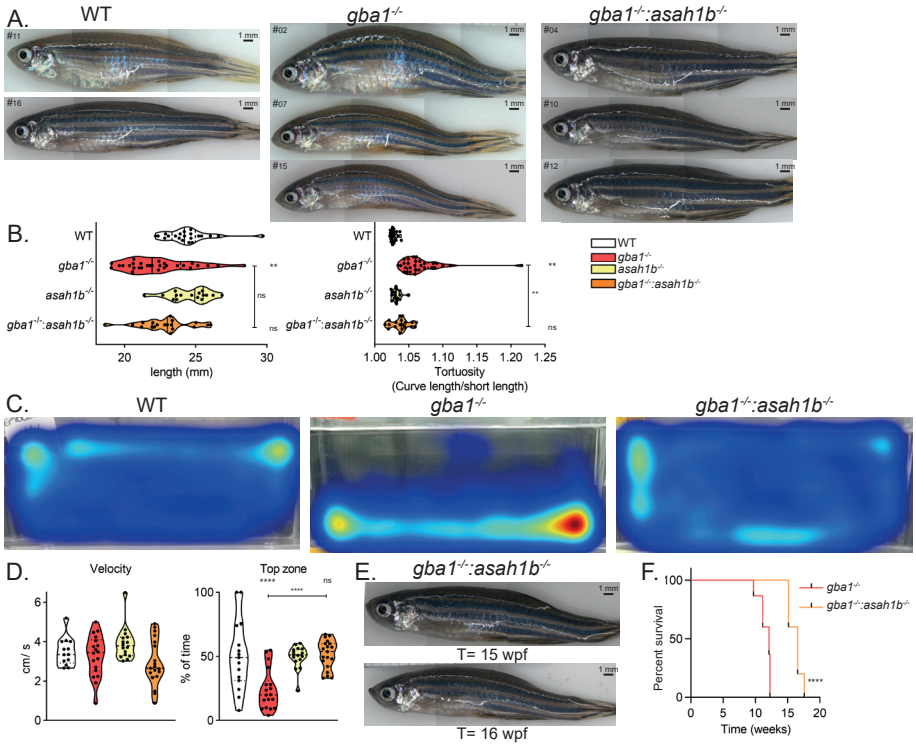

Figure 7 | Phenotypic improvements of adult Asah1b:Gba1 double deficient zebrafish
(A) Representative photographs of WT, *gba1*$^{-/-}$ and *gba1*$^{-/-}$*:asah1b*$^{-/-}$ zebrafish. **(B)** The length of individual zebrafish is determined (head to tail base) as well as the tortuosity, calculated as ratio of the length along the back divided by the length of the fish, as indication for the curved back. Data of individual zebrafish is depicted in a violin plot; WT (n = 21), *gba1*$^{-/-}$ (n = 29), *asah1b*$^{-/-}$ (n = 16), *gba1*$^{-/-}$*:asah1b*$^{-/-}$ (n = 19), and analysed using a non-parametric Kruskal-Wallis test with Dunn's multiple comparison test. **(C)** Representative movement traces of WT, *gba1*$^{-/-}$ and *gba1*$^{-/-}$*:asah1b*$^{-/-}$ zebrafish, all at t = 12 wpf. **(D)** Quantification of individual zebrafish average velocity (in cm/s) and time spend in the top half of the tank. Data of individual zebrafish is depicted in a violin plot; WT (n = 13), *gba1*$^{-/-}$ (n = 16), *asah1b*$^{-/-}$ (n = 16), *gba1*$^{-/-}$*:asah1b*$^{-/-}$ (n = 19) and analysed using a One-Way Anova with Tukey's multiple comparison test. **(E)** Photograph of individual *gba1*$^{-/-}$*:asah1b*$^{-/-}$ zebrafish at t = 15 and 16 wpf. (F) Kaplan-Meier plot indicating the onset of predetermined symptoms, such as the curved back and abnormal swimming resulting in impaired feeding behaviour, of *gba1*$^{-/-}$ and *gba1*$^{-/-}$*:asah1b*$^{-/-}$ zebrafish; *gba1*$^{-/-}$ (n = 30), *gba1*$^{-/-}$*:asah1b*$^{-/-}$ (n = 5). Curves are analysed using a Log-rank (Mantel-Cos) test. In general, statistical comparisons are depicted as WT vs *gba1*$^{-/-}$, WT vs *gba1*$^{-/-}$*:asah1b*$^{-/-}$ or *gba1*$^{-/-}$ vs *gba1*$^{-/-}$*:asah1b*$^{-/-}$, only when a significant difference is apparent and relevant. Ns = not significant, ** P < 0.01 and **** P < 0.0001.

Discussion

The role of GlcSph in GD pathophysiology is still largely based on circumstantial evidence and therefore tentative. The present study describes the generation of a unique GD zebrafish model that sheds light on the importance of GlcSph in pathology. Zebrafish express two ACase enzymes, Asah1a and Asah1b. Only the combined deficiency of both ACases was found to cause marked accumulation of Cer, as occurs in Farber disease, while only Asah1b was found to be involved in the formation of excessive GlcSph during GCase deficiency in zebrafish. The comparison of adult *gba1*$^{-/-}$ fish, with excessive GlcSph, and *gba1*$^{-/-}$*:asah1b*$^{-/-}$ fish, without GlcSph, therefore allows delineation of the contribution of this lyso-lipid to different mechanisms underlying GD manifestations, including storage cells, inflammation and autophagy.

Both *gba1*$^{-/-}$ and *gba1*$^{-/-}$*:asah1b*$^{-/-}$ fish show accumulation of Gaucher-like cells which is accompanied by excessive tissue GlcCer levels. The observation that tissue GlcCer is similar in *gba1*$^{-/-}$ fish and *gba1*$^{-/-}$*:asah1b*$^{-/-}$ fish indicates that ACase-mediated GlcSph formation reduces marginally GlcCer accumulation during GCase deficiency. Despite the GlcCer accumulation and Gaucher-like cells in brain and liver in both GCase deficient fish, a very marked increase in life span is observed for the *gba1*$^{-/-}$*:asah1b*$^{-/-}$ fish. Individual *gba1*$^{-/-}$ zebrafish show a drop of the tail around 8-9 wpf, which progresses in subsequent weeks to a characteristic phenotype of a curved back, postural imbalance and more time spent at the bottom of the tank. No curved back nor abnormalities in swimming behaviour develop in *gba1*$^{-/-}$*:asah1b*$^{-/-}$ fish at 12 wpf and animals live up to 33% longer until similar manifestations to those of *gba1*$^{-/-}$ fish are apparent.

It is tempting to attribute the delayed onset of abnormalities to the absence of GlcSph in GCase-deficient zebrafish lacking ACase-Asah1b. Of note, the absence of GlcSph and improved phenotype was not accompanied by changes in biomarkers of Gaucher cells. The comparably increased expression of mRNAs encoding Gpnmb and Chia.6 in both GCase mutants suggests that similar amounts of lipid-laden macrophages develop in *gba1*$^{-/-}$ fish and *gba1*$^{-/-}$*:asah1b*$^{-/-}$ zebrafish and that the cells react similarly to lysosomal accumulation of GlcCer by increased production of gpNMB and chitinase proteins. Furthermore, increased autophagy occurs in brains of both types of mutant zebrafish, as well as comparable neuroinflammation, as depicted by increased expression of inflammation markers Il-1*β*, Tnf-β and ApoEb and the lysosomal protease Cathepsin D in brains of both *gba1*$^{-/-}$ fish and *gba1*$^{-/-}$*:asah1b*$^{-/-}$ fish. Transcript levels of components of the complement system (*c1qA*, *c3.1*, *c5* and the c5a receptor (*c5aR1*)) are comparably increased in *gba1*$^{-/-}$ and *gba1*$^{-/-}$*:asah1b*$^{-/-}$ brains. In addition, infiltration of Gaucher-like cells in the periventricular grey zone of the optic tectum of the brain is apparent in both *gba1*$^{-/-}$ and *gba1*$^{-/-}$*:asah1b*$^{-/-}$ fish. It will be of interest to comparatively visualize and quantify more closely microglia in brains of the mutant fish. Altogether, the biochemical findings and pathology examination suggest that the presence of excessive GlcSph is not a prerequisite for inflammation.

The considered activation of the complement cascade as major driver of the inflammatory pathology in GD mice[34] was not apparent in our study. Brains of *gba1*$^{-/-}$*:asah1b*$^{-/-}$ fish without excessive GlcSph and no apparent phenotype at that time-point, showed comparable complement activation, compared to phenotypic *gba1*$^{-/-}$ fish of 10-12 wpf. Likewise, impaired autophagy and neuroinflammation did not differ among the GCase-deficient fish with or without excessive GlcSph. Apparently, these processes do not explain the more severe phenotype of GCase-deficient fish with excessive lyso-lipid.

In view of the recently recognized link between mutations in GBA gene and risk for Parkinson disease[35], the fate of dopaminergic neurons in GCase-deficient fish with or without excessive GlcSph is of interest. The expression of mRNAs encoding tyrosine hydroxylase 1 (*th1*), a marker for dopaminergic neurons, is reduced in *gba1*$^{-/-}$ zebrafish brains, but not *gba1*$^{-/-}$*:asah1b*$^{-/-}$ brains. Zebrafish do not encode an orthologue of human α-synuclein, but instead express β-synuclein (*sncβ*) and two γ-synuclein variants (*sncγa* and *sncγb*). The β-synuclein and γ1-synuclein (*sncγb* gene) isoforms are expressed in the cell bodies of TH-positive catecholaminergic cell groups[36]. Two transcripts of zebrafish synucleins, *sncβ* and *sncγb*, were significantly reduced in *gba1*$^{-/-}$ brains compared to WT and *gba1*$^{-/-}$*:asah1b*$^{-/-}$ brains, while the expression of myelin-basic protein (*mbpa*) is comparably reduced in both *gba1* KO and *gba1:asah1b* KO brains. These findings suggest that the presence of excessive GlcSph might specifically impact dopaminergic neurons. However, visualization and quantification of TH-positive dopamine neurons is required to confirm this. Keatinge and colleagues observed earlier in *gba1*$^{-/-}$ zebrafish, a reduction of TH-immunoreactive neurons in the caudal hypothalamus and posterior tuberculum accompanied by abundant Lewy body-like ubiquitinylated neuronal cytoplasmic inclusions and neurites in the hindbrain[30]. In addition, a reduction of β- and γ1-synuclein (*sncgb* gene) protein levels was found. Based on our findings regarding mRNA levels, *gba1*$^{-/-}$*:asah1b*$^{-/-}$ brains lacking excessive GlcSph would likely show a more moderate reduction of TH-immunoreactive neurons. It was earlier observed with GD/PD mouse models that GlcCer levels are not increased in the brain, while GlcSph accumulation already occurs in young mice (8-12 weeks), supposedly triggering α-synuclein aggregation[11]. Similar observations were made with cultured human neuronal cells[11]. In addition, a recent study with mice heterozygous for GBA deficiency showed development of α-synucleinopathy concomitantly to overproduction of GlcSph[10]. These observations all point to a detrimental role of excessive GlcSph regarding dopaminergic neurons. Our findings with zebrafish are in line with this. Further research is required to elucidate the exact role of GlcSph in the accelerated neuronal cell death in the α-synuclein independent zebrafish model. In this connection the proposed harmful effects of complement-activating immune complexes deposited on neuronal cells, oxidative damage and mitochondrial dysfunction[30,37-39] warrant specific attention. Obviously, the absence of α-synuclein in zebrafish, and the different location of dopaminergic neurons as compared to human brain, could limit their use as genuine models to study Parkinson's disease during GBA deficiency[27,30]. More attractive to some extent are *Oryzias latipes* (medaka) fish expressing endogenous α-synuclein[32].

It is important point out that despite delayed disease manifestations and improved life span, *gba1*$^{-/-}$*:asah1b*$^{-/-}$ lacking GlcSph still developed abnormal swimming behaviour at 4 months of age and are culled earlier than WT and *asah1b*$^{-/-}$ age-mates. This suggests that GlcSph contributes significantly to the onset of GD symptoms, but is not the only pathogenic factor. In this respect, the impact of accumulating GlcCer and other glucosylated lipids deserves further attention.

The noted differences between the enzymes encoded by *asah1a* and *asah1b* warrant further discussion. Both ACases hydrolyse ceramide and no abnormal phenotype is observed for fish lacking only one of the ACase enzymes, up to the moderately old age of 2 years. Both *asah1a*$^{-/-}$*:asah1b*$^{+/-}$ and *asah1a*$^{+/-}$*:asah1b*$^{-/-}$ adult zebrafish were obtained at predicted Mendelian frequency, however no adult double *asah1a*$^{-/-}$*:asah1b*$^{-/-}$ zebrafish could be raised. This suggests that maternal ACase in the developing larvae is essential during combined Asah1a and Asah1b deficiency. Moreover, after 5 dpf endogenous ACase activity, either Asah1a or Asah1b, is important for viability. The sequence alignment of Asah1a, Asah1b and human ACase shows a high conservation of relevant residues (**Figure 1**). It is known for human ACase that autocleavage of the peptide bond preceding Cys 143 results in activation of the proenzyme and subsequently leads to a conformational change of Tyr 137[22], a residue also conserved in both Asah1a and Asah1b. Tyr 137 is then stabilized through hydrogen bonding or hydrophobic interactions between the α-subunit helix (residues 127-140) and β-subunit region (residues 225-250, **Supplementary Figure 5**). The conformational change opens up a hydrophobic pocket hosting the fatty acid of ceramide, as implied by the binding conformation of covalent inhibitor Carmofur[23]. Simple molecular modelling of human and zebrafish enzymes, reveals that Asah1a contains more aromatic residues lining the entrance of the pocket (**Supplementary Figure 6**). However, none of these residues seem to be in close proximity to the proposed catalytic site. Residues Asp 200, Phe 201 and Met 300 located on the loops adjacent to the catalytic site might be close enough to be of significance, assuming that these loops adapt a slightly different orientation towards the catalytic site in solution, in comparison to the crystal structures. Nonetheless, whether these residues provide an explanation for the different substrate specificity of Asah1a and Asah1b remains yet unclear. An alternative explanation for our findings could be that Asah1a is less abundant in lysosomes of macrophages in zebrafish, the most likely source of GlcSph formation. Overall, it will be of interest to elucidate in the future why Asah1a is not able to generate GlcSph in GCase-deficient fish.

The ACase-mediated formation of deacylated sphingolipid bases from lipids accumulating in lysosomes is not unique to GD. A similar phenomenon is observed with other lysosomal sphingolipidoses: Fabry disease with globotriaosylsphingosine (lysoGb3) formed from accumulating globotriaosylceramide (Gb3); Krabbe disease with galactosylsphingosine (GalSph) formed from galactosylceramide; acid sphingomyelinase deficiency, a.k.a. Niemann-Pick disease types A and B, with phosphocholinesphingosine formed from sphingomyelin[40,41]. As for GlcSph in GD disease, research has been focused on evaluating the neurotoxic actions of lysoGb3 in Fabry disease and galactosylsphingosine in Krabbe disease[42-45]. Recently, ablation of ACase in a mouse model of Krabbe disease, deficient in

galactocerebrosidase (GALC) showed no GalSph accumulation in brain, liver and spleen tissue[42]. As a result, a reduction of activated macrophages/microglia in the cerebellum was observed as well as improved axonal structures, few infiltrating inflammatory cells, little oedema, improved motor activity and increased life span compared to GALC deficient mice. On the other hand, increased levels of ceramide were apparent in liver and spleen of the GALC/ACase deficient mice as well as haematological abnormalities such as vacuoles in the spleen, circulating monocyte and neutrophil populations, as observed in the ACase deficient mice[42]. The established Asah1b deficient zebrafish without ceramide accumulation could offer interesting opportunities to investigate the detrimental role of deacylated sphingolipid bases in the outcome of other lysosomal storage diseases, without the accompanying ceramide accumulation.

With the improved life span, it is tempting to consider inhibition of ACase as therapeutic avenue in neuronopathic GD with unmet need. Carmofur is a known inhibitor of ACase[46,47]. It has been earlier demonstrated that Carmofur treatment of GCase-deficient cells reduces formation of GlcSph[16]. The compound Carmofur is however not a specific ACase inhibitor, as it also inactivates neutral ceramidases and it is known to inhibit the nucleotide-synthesizing enzyme thymidylate synthetase, an effect underlying its wide-spread use in chemotherapy[46]. More specific ACase inhibitors have been designed by Fabrias and colleagues[48]. Testing such compounds in our zebrafish models of GCase deficiency could be considered as first step to assess clinical applicability. The window for such type of intervention might be very small, or even not exist, given the report that partial ACase deficiency already impairs spinal-cord motor neurons and other areas of the CNS[49].

In conclusion, the comparison of GCase-deficient zebrafish with or without excessive GlcSph, due to respective presence or absence of Asah1b, reveals that the latter fish show amelioration of swimming abnormalities and increased life span. It is remarkable that this improvement in disease manifestations in the absence of GlcSph is independent of storage cell burden and neuroinflammation.

Acknowledgements

Joost Willemse is kindly acknowledged for the ImageJ plugin to quantify the length and tortuosity of individual zebrafish. Wouter Bax is kindly acknowledged for his work on studying zebrafish Asah1a and Asah1b in vitro and Ulrike Nehrdich, Guus van der Velden and Ruth van Koppen for their overall expertise and particularly for their help in monitoring the mutant zebrafish. The study was supported by the NWO BBOL 2018 (737.016.022) grant.

Supplementary Information

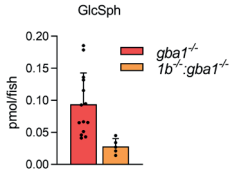

Supplementary Figure 1 | GlcSph levels of gba1$^{-/-}$ (n = 14) and *gba1*$^{-/-}$*:asah1b*$^{-/-}$ (n = 5) larvae KO at 5dpf in pmol/fish. Data of *gba1*$^{-/-}$ is used from chapter 5. Data is depicted as mean ± SD.

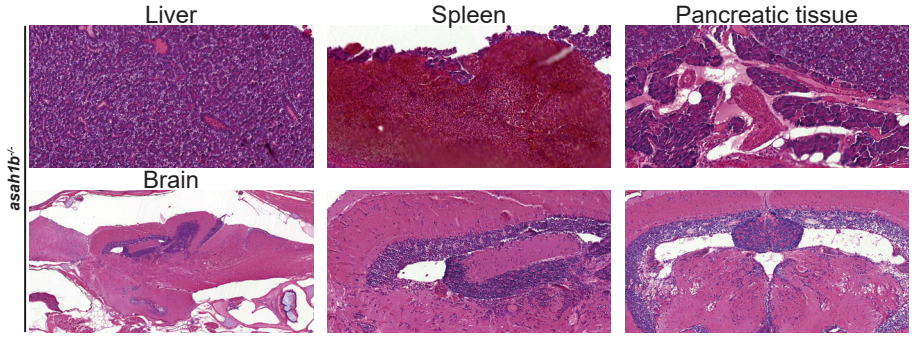

Supplementary Figure 2 | H&E staining of *asah1b*$^{-/-}$ zebrafish including liver, spleen and pancreatic tissue as well as sagittal section (left and magnification in the middle panel) and transversal section (right panel) of *asah1b*$^{-/-}$ zebrafish brain.

asah1b$^{-/-}$*:gba1*$^{+/+}$

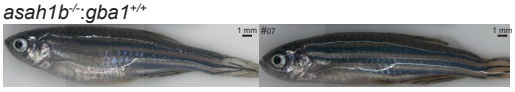

Supplementary Figure 3 | Photographs of two representative *asah1b*$^{-/-}$ zebrafish.

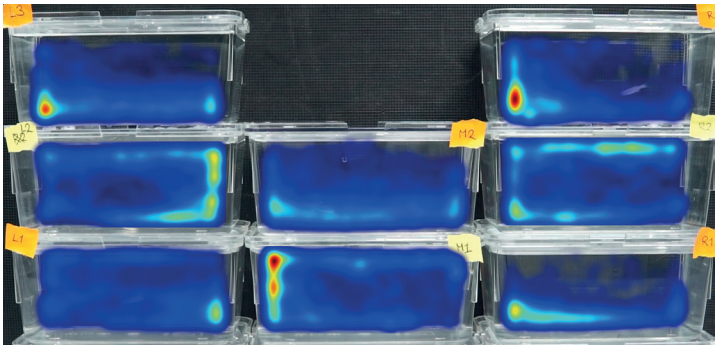

Supplementary Figure 4 | Heatmaps of individually filmed zebrafish at 15 wpf.
Heatmaps of *asah1b*$^{-/-}$ (yellow stickers) and *gba1*$^{-/-}$*:asah1b*$^{-/-}$ (orange stickers) at 15 wpf, with individual fish starting to show differences in swimming behaviour. Red indicates more time and blue less time spend at that location.

```
Human ACase     MPGRSCVALV-LLAAAVSCAVAQHAPPWTEDCRKSTYPPSGPTYRGAVPWYTINLDLPPY      59
Asah1a          ----MKLVFRYNALFISIFIHALYV-QGLEDCRSGMYPPKGPTYRGNVTRYTVNLDLPPS      55
Asah1b          MNNRLNLCFFI-LSYMCMCLSAQYVPPFTEDCRSGMYPPNGPTFKGDVSWYTVDLDLPAS      59
                          : :             * :.    ****.. ***.***::* *  **::****

Human ACase     KRWHELMLDKAPVLKVIVNSLKNMINTFVPSGKIMQVVDEKLPGLLGNFPGPFEEEMKGI      119
Asah1a          ERWTQIIKDKNTELIEMVQTIKDMAKGFF-HGKLVNFVDKELPFIVDTLPNPFNEEIKGI      114
Asah1b          KRWTDVISDKKTEMASMIQAIRDLADAFVPSGKLIQLVDKDLPLMVDTLPYPFNEEIRGI      119
                :** ::: **   : :::::::: . *.  **:::.**:.** ::..:* **:**::**
                                α-subunit helix

Human ACase     AAVTDIPLGEIISFNIFYELFTICTSIVAEDKKGHLIHGRNMDFGVFLGWNINNDTWVIT      179
Asah1a          AAVSGIPLGEIALFNIFYEVFTVCTSLVAEDNNGNIYHGRNLDFGLFMGWDRQNKTWTLT      174
Asah1b          ASVSGVPLGEVVLFNIFYEVFTVCTSLVAEDVNGNLIHARNLDFGLFMGWDLKNRSWVIT      179
                *:*:.:****:  ******:**:***:**** :*:: *.**:***:*:**: :* :*.:*
                                                          β-subunit region

Human ACase     EQLKPLTVNLDFQRNNKTVFKASSFAGYVGMLTGFKPGLFSLTLNERFSINGGYLGILEW      239
Asah1a          EKLKPLVVNINFERKNQTVFKSTSFAGYVGMLTGIRPGELTLTMNERFDFDGGYIGILDW      234
Asah1b          EKLKPLVVNIDFTRNGQTVFKSTNFAGYVGMLTGIHQNSFTLTMNERFSLDGGYIGILEW      239
                *:****.**::* *:.:****::.********** . ::**:****.::***:***:*

Human ACase     ILGKKDVMWIGFLTRTVLENSTSYEEAKNLLTKTKILAPAYFILGGNQSGEGCVITRDRK      299
Asah1a          IFGNRDGMWTGFLTRRVLENSTSYEDAKDQLSQTKLLAPVYFILGGNRTGQGCVITRTRI      294
Asah1b          ILGKRDGMWMSFLTRSVLENATSYESAKALLSDTKLLAPAYFILGGNQSGEACIITRSRT      299
                *:*::* ** .**** **** :****.** *:.**:***.********::*:.*:*** *

Human ACase     ESLDVYELDAKQGRWYVVQTNYDRWKHPFFLDDRRTPAKMCLNRTSQENISFETMYDVLS      359
Asah1a          NTLDIWELELMLGRWYVLETNYDHWDKPMFLDDRRTPAMKCMNQTTQANISLASIYNVLS      354
Asah1b          QNISPLELNVKNGRWYVLETNYDHWKEPLFLDDRRTPAMKCMNQTTQTNISVKTVYDVLS      359
                :.:.  **:   *****::****:*..*:********  *:*:*:* ***. ::*:***

Human ACase     TKPVLNKLTVYTTLIDVTKGQFETYLRDCPDPCIGW 395
Asah1a          TKPVLNKLTTYTSLMAVSTGTLESYVRDCPNPCTPW 390
Asah1b          TKPVLNKLTTYTTLMEVSKGTLESFIRDCPNPCMPW 395
                *********.**:*: *:.* :*:::****:**  *
```

Supplementary Figure 5 | Sequence alignment of acid ceramidase variants with the predicted signal peptide (depicted in blue), self-cleaved catalytic residue C143 (bold, red) and contrasting residues (highlighted in grey). Modelled residues indicated with black line above while residues D200, F201 and M300 of Asah1a are indicated in bold.

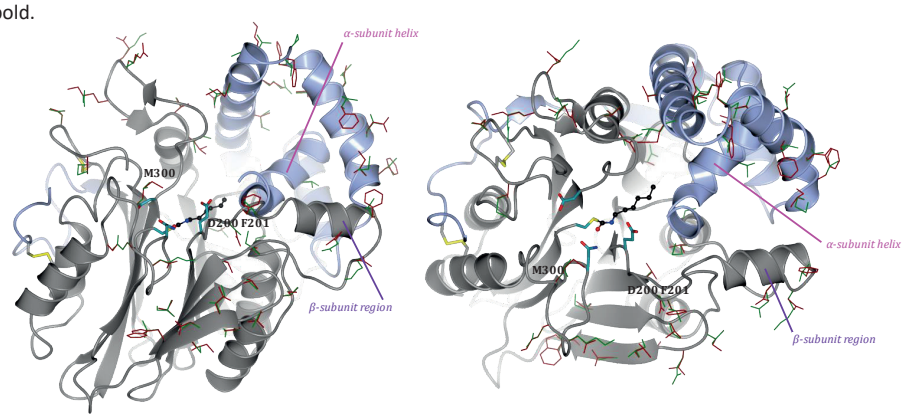

Supplementary Figure 6 | Structure of human ACase with modelling of divergent residues of Asah1a and Asah1b
Ribbon diagram of the side (left) or top (right) of human ACase (PDB 6MHM) with α-subunit (light grey), β-subunit (dark grey) and disulfide bonds (yellow) indicated. Inhibitor Carmofur (black, ball and stick) and catalytic residues C143, D162, E225 or N320 (cyan sticks) are also visualized for clarity, as proposed by Dementiev et al.[23]. Divergent residues of Asah1a (red) and Asah11b (green) surrounding the catalytic pocket are superimposed on the human structure.

Experimental procedures

Chemicals and reagents - GCase specific inhibitor (ME656)[27], $^{13}C_5$-sphinganine, $^{13}C_5$-sphingosine, $^{13}C_5$-GlcSph, $^{13}C_5$-lyso-globotriaosylceramide (LysoGb3), C17-lysosphingo-myelin (LysoSM), $^{13}C_6$-GlcChol and C17-dihydroceramide (C17-dhCer)[50,51] were synthesized as reported. All chemicals and reagents were obtained from Sigma-Aldrich Chemie Gmbh (St Louis, USA) unless mentioned otherwise. The standards Cer (d18:1/16:0), dhCer (d18:0/16:0), GlcCer (d18:1/16:0), GalCer (d18:1/16:0), LacCer (d18:1/16:0) were obtained from Avanti Polar lipids (Alabaster, USA) and GlcChol from Sigma-Aldrich. LC-MS grade methanol, 2-propanol, water, formic acid, acetonitrile and HPLC grade chloroform were purchased from Biosolve (Valkenswaard, the Netherlands). LC-MS grade ammonium formate, ammonium acetate and sodium hydroxide from Sigma-Aldrich, butanol and hydrochloric acid from Merck Millipore (Billerica, USA).

Zebrafish - All zebrafish were housed and maintained at the University of Leiden, the Netherlands, according to standard protocols. Wildtype (WT) zebrafish (ABTL) were a mixed lineage of WT AB and WT TL genetic backgrounds. Zebrafish were kept at constant temperature of 28.5 °C and on a cycle of 14-hour light and 10 hour dark. Experiments with larvae, juvenile and adult zebrafish after the free-feeding stage were approved by the local animal welfare committee (Instantie voor Dierwelzijn) of the University Leiden (Project license AVD1060020184725). Zebrafish from 5 dpf to 2 wpf were fed with both dry food (2x daily; Skretting Gemma micro 75, Zebcare, Nederweert, the Netherlands) and Rotifers (1x daily) and from 3 wpf to the end of the experiment fed with both dry food (2x daily; Skretting Gemma micro 150 until 30 dpf or Gemma Micro 300 mixed with Gemma Diamond for fish from 30 dpf) and hatched Artemia (1x daily).

Zebrafish sampling, morphology and movement - In general, zebrafish were sacrificed at 12 wpf or earlier when zebrafish showed symptoms noted as human endpoints in the project license (t = 10-11 wpf for *gba1*$^{-/-}$). Zebrafish (10-12 wpf) were recorded individually from the side for 20 minutes, after 10 minutes of acclimatization in their new tank. Movements of the fish in the individual tank was tracked using Ethiovision software 10.1 (Noldus, Wageningen, the Netherlands). Arenas were setup for each individual tank, with a division for the top and bottom zone, and subsequently data was obtained for 10 minutes. Fish were subsequently sacrificed using an overdose of tricaine methane sulfonate (MS222, 200 mg/L) and photographed using Leica M165C (Wetzlar, Germany). The three or four images of one fish were stitched to obtain one image using Photoshop CC2018 (Adobe, San Jose, USA) The length of the fish from head to tail base (short length) was determined as well as the length of the back from head to tail base (long length) using ImageJ software[52]. The tortuosity was calculated by dividing the long length by the short length. Whole zebrafish were fixed using paraformaldehyde (4% (w/v), Alfa Aesar, Haverhill, USA) or Bouin's solution (5% acetic acid, 9% formaldehyde, 0.9% picric acid, Sigma) for histopathology performed as described below or organs were dissected. Dissected organs were either snap frozen for protein and (glyco)sphingolipid analysis or submerged in RNAlater™ (Invitrogen, Thermo Fisher Scientific, Waltham USA) for RT-PCR analysis (brain or liver) and stored at -80 °C.

CRISPR/Cas9 mediated knockout of *asah1a* and *asah1b* - CRISPR/Cas9 mediated *gba1* knockout zebrafish were generated and maintained as previously described[26]. CRISPR/Cas9 mediated zebrafish gene knockouts of *asah1a* and *asah1b* were generated using the protocol previously described (Chapter 4 and[26] with sgRNA1 5'-gGTGTCCATCTCTCACTAGG and sgRNA2 5'-GgGCTTCCCG CTGGGAACAA for *asah1a* and *asah1b* respectively. Of note, the first or second nucleotide of the sgRNA found by the CHOPCHOP webtool was replaced by a 'g' to improve T7 RNA synthesis. Injected founders were crossed to WT and off-spring screened using an HRM assay with primers described in **Supplementary Table 1**. Fragments for Sanger sequencing were obtained using primers described in **Supplementary Table 1**. Heterozygous adult zebrafish (F2 generation) of both genotypes were crossed to obtain double heterozygous zebrafish (*asah1a*$^{+/-}$:*asah1b*$^{+/-}$). Adult fish were crossed with

each other and off-spring was used for incubations with vehicle (0.1% DMSO) or GCase specific inhibitor (10 µM ME656, 0.1% DMSO) for 5 days, followed by (glyco)sphingolipid analysis. The *gba1*$^{-/-}$, *gba1*$^{+/+}$*:asah1b*$^{-/-}$ and *gba1*$^{-/-}$*:asah1b*$^{-/-}$ zebrafish were generated by appropriate crossings. The status of *gba1* and *asah1b* was determined by fin clipping of 4-5 dpf larvae and subsequent HRM assays.

Supplementary Table 1| Forward (F) and reverse (R) primers for HRM analysis and amplification for sequencing

Target	Sequence 5'->3'	Target	Sequence 5'->3'
Asah1a HRM F	GTCTAGACTCGAATAAGTTCATG	*Asah1a* sequencing F	TGGGATGTATCCACCTAAAGG
Asah1a HRM R	TGGGAAACAGTTACCTCTGTG	*Asah1a* sequencing R	Same as HRM R
Asah1b HRM F	TGCAAAGAGATGTGTTAGATTG	*Asah1b* sequencing F	CAGCAAGCAAAAGATGGACAG
Asah1b HRM R	TCCTTCAGATGGCGAGCATG	*Asah1b* sequencing R	TACGATTTTGGGAGATTTATCTC

Homogenate preparation - Homogenates of organs were prepared in potassium phosphate lysis buffer (25 mM K_2HPO_4-KH_2PO_4 pH 6.5, 0.1% (v/v) Triton-X100 and EDTA-free protease inhibitor (cOmplete™, EDTA-free Protease Inhibitor Cocktail, Roche, Sigma-Aldrich)). Organs were first homogenized using a Dounce homogenizer (10 strokes) followed by sonication (20% amplitude, 3 sec on, 3 sec off for 4 cycles) using a Vibra-Cell™ VCX 130 (Sonics, Newtown, USA) while on ice. Total protein concentration of homogenates was determined using Pierce™ BCA protein assay kit (Thermo Fisher Scientific, Waltham, USA) and measured using an EMax® plus microplate reader (Molecular Devices, Sunnyvale, USA).

Western blot - Proteins of organ homogenates (20 µg protein) were denatured using 5x Laemmli sample buffer (25% (v/v) 1.25M Tris-HCL pH 6.8, 50% (v/v) 100% glycerol, 10% (w/v) sodium dodecyl sulphate (SDS), 8% (w/v) dithiothreitol (DTT) and 0.1% (w/v) bromophenol blue), samples were boiled for 5 min at 98 °C and proteins were separated by electrophoresis on a 12% (w/v) SDS-PAGE gel. Proteins were transferred to nitrocellulose membranes (0.2 µM, Bio-Rad laboratories Inc., Hercules, USA) using the Trans-Blot® Turbo™ Transfer system (Bio-Rad). Membranes were blocked with 5% (w/v) bovine albumin serum (BSA) and incubated overnight at 4 °C with primary antibodies: rabbit anti-LC3 (1:1000, NB100-2220; Novus Biologicals, Centennial, USA), rabbit anti-p62/SQSTM1 (1:1000, P0067; Sigma) or rabbit anti-actin (1:1000, ab209857; Abcam, Cambridge, UK). Membranes were washed 3 times with TBST and incubated for 1 h at RT with secondary antibody: GARPO goat anti rabbit IgG (H+L) peroxidase (1:5000, Bio-Rad). Chemiluminescence signal is developed using the Clarity Max Western ECL substrate (Bio-Rad), detected using a ChemiDocMP imager (Bio-Rad) and signal quantified by ImageJ software.

Gene expression analysis - RNAlater™ was removed and RNA was extracted using a Nucleospin RNA XS column (Machinery-Nagel, Düren, Germany) procedure according to supplier's protocol, without the addition of carrier RNA. Contaminating DNA was degraded on column by a DNase I treatment (supplied in the kit). cDNA was synthesized using SuperScript™ II reverse transcriptase (Invitrogen, ThermoFisher Scientific, Waltham, USA) using oligo(dT) and an input of approximately 200-500 ng total RNA according to the manufacturer's instruction. Generated cDNA was diluted to an approximate concentration of 0.5 ng total RNA input/µL with Milli-Q water. RT-PCR reactions were performed with the IQ SYBR green mastermix (Bio-Rad laboratories Inc., Hercules, USA) in a total volume of 15 µL (1x SYBR green, 333 µM of forward and reverse primer as given in Supplementary Table 2 and 5 µL of the diluted cDNA input) and carried out using a CFX96™ Real-Time PCR Detection system (Bio-Rad laboratories Inc., Hercules, USA) with the following conditions: denaturation at 95 °C for 3 min, followed by 40 cycles of amplification (95 °C for 30 sec and 61 °C for 30 sec), imaging the plate after every extension at 61 °C, followed by a melt program from 55-95 °C with 0.5 °C per step with imaging the plate every step. All biological samples were tested in technical duplicate, differential gene expression was calculated using the ΔΔCτ method normalized to two house-keeping genes *ef1a* and *rpl13* and depicted as $\log_2$ fold change ± SEM, compared to WT.

Supplementary Table 2| Forward and reverse primers for RT-qPCR analysis.

Target	NCBI code	Forward primer sequence (5'->3')	Reverse primer sequence (5'->3')	
Asah1a	NM_001006088	ATTAGGCCTGGTGAACTGAC	CTGCGAGTAAGAAAACCCGTC	125 bp
Asah1b	NM_200577	TGGACTGTTCATGGGATGGG	CCGGTCAACATCCCGACATA	150 bp
Gpnmb	XM_009294247	GCAAGGGCGTAGAATTGAAA	TGGCAGGGACATGTCAGTAA	
Chia.6	NM_199603	TCCACGGCTCATGGGAGAGTGTC	AGCGCCCTGATCTCGCCAGT	ref. 53
catD	NM_131710	TGGGTGGAAAGGTCTACTCG	CACTCAGGCAGATGTCGTGT	
il1β	NM_212844	TGGACTTCGCAGCACAAAATG	GTTCACTTCACGCTCTTGGATG	ref. 54
tnfβ	NM_182873	GCATGTGATGAAGCCAAACG	GATTGTCCTGAAGGGTCACC	ref. 55
apoeb	NM_131098	AAACTGACATGACCGACGCT	TAGGTTGCTACGGTGTTGCG	172 bp
c1qA	NM_001020527	CTCTGTTTCCCTTTTCCTTCTG	CTTTCTCTCCTTTTGGTCCTGG	108 bp
c3a.1	NM_131242	CGCTGCACAAAGTACTTCCAC	GCCAGCTCCATGTCCTTGAC	197 bp
c5aR1	XM_005159274	CCGACAAGCTCGCATCCTAT	GCGAATGATGGTTATCGCCC	163 bp
c5	XM_001919191	CAAGGCCACGGTTCAATCAG	TCTTCATGCTTTCGGCAGTCA	152 bp
th1	NM_131149	AGCTTTGTGGACGCTACTGA	GTGGGTTGTCCAGCACTTCT	112 bp
th2	NM_001001829	TACAAGCCATTCGACCCAGC	ATGCTGCAAGTGTAGGGGTC	173 bp
sncβ	NM_200969	GGAGTTTGGTCAGGAAGCCA	CCTCGGGCTCATAATCCTGG	107 bp
sncγa	NM_001017567	TGGAGGGGCTGGAGACTATG	AGCATCATGGGACATTCGGTT	123 bp
sncγb	NM_001020652	ATGGTGAACCCGGGTGACTT	AGGCTTTGGAGCAGAAACGTA	129 bp
mcpa	XM_002665562	TGGTCATCTATCCTCCTCTCCA	CTTTCTCCCAGGCCCAATAGTTCT	150 bp
ef1a		CTGGAGGCCAGCTCAAACAT	ATCAAGAAGAGTAGTACCGCTAGCATTAC	ref. 56
rpl13α		TCTGGAGGACTGTAAGAGGTATGC	AGACGCACAATCTTGAGAGCAG	ref. 56

(Glyco)sphingolipid analysis - Neutral (glyco)lipids, (glyco)sphingoid bases and glycosylated cholesterol were extracted from the same homogenate (10 µL, 20-30 µg total protein in KPi lysis buffer) using an acidic Bligh and Dyer procedure (1/1/0.9 chloroform/methanol/100 mM formate buffer pH 3.1) as described before[26,51]. Lipids were resuspended in methanol for separation by a C18 column or acetonitrile/methanol (9/1, v/v) for separation using a HILIC column and transferred to a vial for LC-MS/MS analysis. LC-MS/MS measurements were performed using a Waters UPLC-Xevo-TQS micro instrument (Waters, Corporation, Milford, USA) in positive mode using an electrospray ionization (ESI) source as described before for separating GlcChol and (glyco)sphingolipids using the C18 column[26,50,51]. To separate lipids by HILIC chromatography, a BEH HILIC column (2.1 x 100 mm with 1.7 µm particle size, Waters) was used at 30 °C as described before[26] with minor modifications in the eluent program allowing a faster run while preserving separation of Glc- and Gal containing lipids. Eluent A contained 10 mM ammonium formate in acetonitrile/water (97:3, v/v) with 0.01% (v/v) formic acid and eluent B consisted of 10 mM ammonium formate in acetonitrile/water (75:15, v/v) with 0.01% (v/v) formic acid. Lyso- and deacylated glycosphingolipids were eluted in 10 min with a flow of 0.6 mL/min using the following program: 85% A from 0-1 min, 85-65% A from 1-2.5 min, 60-0% A from 2.5-4 min, 0% A from 4-4.5, 0-85% A from 4.5-4.6 min and re-equilibration with 85% A from 4.6-10 min. GlcChol was eluted in 18 min with a flow of 0.25 ml/min using the following program: 100% A from 0-3 min, 100-0 % A from 3-3.5 min, 0 % A from 3.5-4.5 min, 0-100 % A from 4.5-5 min and re-equilibration with 100 % A from 5-18 min. Lipid levels were calculated in pmol/mg total protein, sphingoid bases and GlcChol were calculated based on the respective isotopic ^{13}C internal standard, while deacylated neutral (glyco)sphingolipids were calculated using C17-dhCer as internal standard and normalized using the respective standard.

Histology - For H&E staining, zebrafish were fixed in paraformaldehyde (4% PFA (w/v), Alfa Aesar, Haverhill, USA) overnight or Bouin's solution (5% acetic acid, 9% formaldehyde, 0.9% picric acid, Sigma) for 4 days, decalcified for 4 days using formic acid (20% (v/v)) and embedded in paraffin. Subsequently, serial sections of 5 µM thickness were made using a Leica RM2055 microtome. Sections were stained with Haematoxylin and Eosin.

Sequence alignment and modelling - Signal peptides were predicted using the SignalP-5.0 server[28] and sequences aligned with Clustal Omega[29]. Signal peptides were excluded and Asah1a or Asah1b structures where modelled with Swiss-Model[57] using human ACase, PDB 6MHM[23], as search model. Structures were superimposed and visualized with CCP4MG[58].

Statistical analyses - Statistical analyses were performed using GraphPad Prism (v8.1.1, GraphPadsoftware, CA, USA) and data depicted as described in the result section. Data of lipid, protein and mRNA levels was analysed by One-Way Anova using Dunnett's test, with WT as control group, or Tukey's multiple comparison test as described in the result section. Data of length and tortuosity are analysed using a non-parametric Kruskal-Wallis test with Dunn's multiple comparison. In general, statistical comparisons are performed of WT vs *gba1*$^{-/-}$, WT vs *gba1*$^{-/-}$*:asah1b*$^{-/-}$and *gba1*$^{-/-}$ vs *gba1*$^{-/-}$*:asah1b*$^{-/-}$, and depicted only when a significant difference is apparent and relevant. Ns = not significant, * $P< 0.05$, ** $P< 0.01$, *** $P< 0.001$ and **** $P< 0.0001$.

References

1. Hollak C.E., van Weely S., van Oers M.H.and Aerts J.M. (1994) Marked elevation of plasma chitotriosidase activity. A novel hallmark of Gaucher disease. *The Journal of clinical investigation* **93**, 1288-1292.
2. Boot R.G., Verhoek M., de Fost M., Hollak C.E., Maas M., Bleijlevens B.,... and Aerts J.M. (2004) Marked elevation of the chemokine CCL18/PARC in Gaucher disease: a novel surrogate marker for assessing therapeutic intervention. *Blood* **103**, 33-39.
3. Kramer G., Wegdam W., Donker-Koopman W., Ottenhoff R., Gaspar P., Verhoek M.,... and van Eijk M. (2016) Elevation of glycoprotein nonmetastatic melanoma protein B in type 1 Gaucher disease patients and mouse models. *FEBS Open Bio* **6**, 902-913.
4. van Dussen L., Hendriks E.J., Groener J.E., Boot R.G., Hollak C.E.and Aerts J.M. (2014) Value of plasma chitotriosidase to assess non-neuronopathic Gaucher disease severity and progression in the era of enzyme replacement therapy. *J Inherit Metab Dis* **37**, 991-1001.
5. Deegan P.B., Moran M.T., McFarlane I., Schofield J.P., Boot R.G., Aerts J.M.and Cox T.M. (2005) Clinical evaluation of chemokine and enzymatic biomarkers of Gaucher disease. *Blood Cells Mol Dis* **35**, 259-267.
6. Murugesan V., Liu J., Yang R., Lin H., Lischuk A., Pastores G.,... and Mistry P.K. (2018) Validating glycoprotein non-metastatic melanoma B (gpNMB, osteoactivin), a new biomarker of Gaucher disease. *Blood Cells Mol Dis* **68**, 47-53.
7. Dekker N., van Dussen L., Hollak C.E., Overkleeft H., Scheij S., Ghauharali K.,... and Aerts J.M. (2011) Elevated plasma glucosylsphingosine in Gaucher disease: relation to phenotype, storage cell markers, and therapeutic response. *Blood* **118**, e118-127.
8. Ferraz M.J., Kallemeijn W.W., Mirzaian M., Herrera Moro D., Marques A., Wisse P.,... and Aerts J.M. (2014) Gaucher disease and Fabry disease: new markers and insights in pathophysiology for two distinct glycosphingolipidoses. *Biochimica et biophysica acta* **1841**, 811-825.
9. Nair S., Boddupalli C.S., Verma R., Liu J., Yang R., Pastores G.M.,... and Dhodapkar M.V. (2015) Type II NKT-TFH cells against Gaucher lipids regulate B-cell immunity and inflammation. *Blood* **125**, 1256-1271.
10. Ikuno M., Yamakado H., Akiyama H., Parajuli L.K., Taguchi K., Hara J.,... and Takahashi R. (2019) GBA haploinsufficiency accelerates alpha-synuclein pathology with altered lipid metabolism in a prodromal model of Parkinson's disease. *Human molecular genetics* **28**, 1894-1904.
11. Taguchi Y.V., Liu J., Ruan J., Pacheco J., Zhang X., Abbasi J.,... and Chandra S.S. (2017) Glucosylsphingosine Promotes alpha-Synuclein Pathology in Mutant GBA-Associated Parkinson's Disease. *J Neurosci* **37**, 9617-9631.
12. Reed M.C., Schiffer C., Heales S., Mehta A.B.and Hughes D.A. (2018) Impact of sphingolipids on osteoblast and osteoclast activity in Gaucher disease. *Mol Genet Metab* **124**, 278-286.
13. Smith N.J., Fuller M., Saville J.T.and Cox T.M. (2018) Reduced cerebral vascularization in experimental neuronopathic Gaucher disease. *J Pathol* **244**, 120-128.
14. Lukas J., Cozma C., Yang F., Kramp G., Meyer A., Nesslauer A.M.,... and Rolfs A. (2017) Glucosylsphingosine Causes Hematological and Visceral Changes in Mice-Evidence for a Pathophysiological Role in Gaucher Disease. *Int J Mol Sci* **18**.
15. Dekker N., Voorn-Brouwer T., Verhoek M., Wennekes T., Narayan R.S., Speijer D.,... and Aerts J.M. (2011) The cytosolic beta-glucosidase GBA3 does not influence type 1 Gaucher disease manifestation. *Blood Cells Mol Dis* **46**, 19-26.
16. Ferraz M.J., Marques A.R., Appelman M.D., Verhoek M., Strijland A., Mirzaian M.,... and Aerts J.M. (2016) Lysosomal glycosphingolipid catabolism by acid ceramidase: formation of glycosphingoid bases during deficiency of glycosidases. *FEBS Lett* **590**, 716-725.
17. Park J.H.and Schuchman E.H. (2006) Acid ceramidase and human disease. *Biochimica et biophysica acta* **1758**, 2133-2138.
18. Yu F.P.S., Amintas S., Levade T.and Medin J.A. (2018) Acid ceramidase deficiency: Farber disease and SMA-PME. *Orphanet J Rare Dis* **13**, 121.
19. Okino N., He X., Gatt S., Sandhoff K., Ito M.and Schuchman E.H. (2003) The reverse activity of human acid ceramidase. *J Biol Chem* **278**, 29948-29953.
20. Bernardo K., Hurwitz R., Zenk T., Desnick R.J., Ferlinz K., Schuchman E.H.and Sandhoff K. (1995) Purification, characterization, and biosynthesis of human acid ceramidase. *J Biol Chem* **270**, 11098-11102.
21. Ferlinz K., Kopal G., Bernardo K., Linke T., Bar J., Breiden B.,... and Sandhoff K. (2001) Human acid ceramidase: processing, glycosylation, and lysosomal targeting. *J Biol Chem* **276**, 35352-35360.
22. Gebai A., Gorelik A., Li Z., Illes K.and Nagar B. (2018) Structural basis for the activation of acid ceramidase. *Nature communications* **9**, 1621.
23. Dementiev A., Joachimiak A., Nguyen H., Gorelik A., Illes K., Shabani S.,... and Doan N. (2019) Molecular Mechanism of Inhibition of Acid Ceramidase by Carmofur. *Journal of medicinal chemistry* **62**, 987-992.

24. Rajput V.B., Karthikeyan M.and Ramasamy S. (2019) Zebrafish acid ceramidase: Expression in Pichia pastoris GS115and biochemical characterization. *Int J Biol Macromol* **122**, 587-593.
25. Zhou J., Tawk M., Tiziano F.D., Veillet J., Bayes M., Nolent F.,... and Melki J. (2012) Spinal muscular atrophy associated with progressive myoclonic epilepsy is caused by mutations in ASAH1. *Am J Hum Genet* **91**, 5-14.
26. Lelieveld L.T., Mirzaian M., Kuo C.L., Artola M., Ferraz M.J., Peter R.E.A.,... and Aerts J. (2019) Role of beta-glucosidase 2 in aberrant glycosphingolipid metabolism: model of glucocerebrosidase deficiency in zebrafish. *J Lipid Res* **60**, 1851-1867.
27. Artola M., Kuo C.L., Lelieveld L.T., Rowland R.J., van der Marel G.A., Codee J.D.C.,... and Overkleeft H.S. (2019) Functionalized Cyclophellitols Are Selective Glucocerebrosidase Inhibitors and Induce a Bona Fide Neuropathic Gaucher Model in Zebrafish. *Journal of the American Chemical Society* **141**, 4214-4218.
28. Almagro Armenteros J.J., Tsirigos K.D., Sonderby C.K., Petersen T.N., Winther O., Brunak S.,... and Nielsen H. (2019) SignalP 5.0 improves signal peptide predictions using deep neural networks. *Nat Biotechnol* **37**, 420-423.
29. Madeira F., Park Y.M., Lee J., Buso N., Gur T., Madhusoodanan N.,... and Lopez R. (2019) The EMBL-EBI search and sequence analysis tools APIs in 2019. *Nucleic acids research* **47**, W636-W641.
30. Keatinge M., Bui H., Menke A., Chen Y.C., Sokol A.M., Bai Q.,... and Bandmann O. (2015) Glucocerebrosidase 1 deficient Danio rerio mirror key pathological aspects of human Gaucher disease and provide evidence of early microglial activation preceding alpha-synuclein-independent neuronal cell death. *Human molecular genetics* **24**, 6640-6652.
31. Menke A.L., Spitsbergen J.M., Wolterbeek A.P.and Woutersen R.A. (2011) Normal anatomy and histology of the adult zebrafish. *Toxicol Pathol* **39**, 759-775.
32. Uemura N., Koike M., Ansai S., Kinoshita M., Ishikawa-Fujiwara T., Matsui H.,... and Takahashi R. (2015) Viable neuronopathic Gaucher disease model in Medaka (Oryzias latipes) displays axonal accumulation of alpha-synuclein. *Plos Genet* **11**, e1005065.
33. Peri F.and Nusslein-Volhard C. (2008) Live imaging of neuronal degradation by microglia reveals a role for v0-ATPase a1 in phagosomal fusion in vivo. *Cell* **133**, 916-927.
34. Pandey M.K., Grabowski G.A.and Kohl J. (2018) An unexpected player in Gaucher disease: The multiple roles of complement in disease development. *Semin Immunol* **37**, 30-42.
35. Sidransky E., Nalls M.A., Aasly J.O., Aharon-Peretz J., Annesi G., Barbosa E.R.,... and Ziegler S.G. (2009) Multicenter analysis of glucocerebrosidase mutations in Parkinson's disease. *N Engl J Med* **361**, 1651-1661.
36. Milanese C., Sager J.J., Bai Q., Farrell T.C., Cannon J.R., Greenamyre J.T.and Burton E.A. (2012) Hypokinesia and reduced dopamine levels in zebrafish lacking beta- and gamma1-synucleins. *J Biol Chem* **287**, 2971-2983.
37. Vitner E.B., Farfel-Becker T., Eilam R., Biton I.and Futerman A.H. (2012) Contribution of brain inflammation to neuronal cell death in neuronopathic forms of Gaucher's disease. *Brain* **135**, 1724-1735.
38. Blesa J., Trigo-Damas I., Quiroga-Varela A.and Jackson-Lewis V.R. (2015) Oxidative stress and Parkinson's disease. *Front Neuroanat* **9**, 91.
39. Pandey M.K., Burrow T.A., Rani R., Martin L.J., Witte D., Setchell K.D.,... and Grabowski G.A. (2017) Complement drives glucosylceramide accumulation and tissue inflammation in Gaucher disease. *Nature* **543**, 108-112.
40. Ferraz M.J., Marques A.R., Gaspar P., Mirzaian M., van Roomen C., Ottenhoff R.,... and Aerts J.M. (2016) Lyso-glycosphingolipid abnormalities in different murine models of lysosomal storage disorders. *Mol Genet Metab* **117**, 186-193.
41. Welford R.W., Garzotti M., Marques Lourenco C., Mengel E., Marquardt T., Reunert J.,... and Groenen P. (2014) Plasma lysosphingomyelin demonstrates great potential as a diagnostic biomarker for Niemann-Pick disease type C in a retrospective study. *PloS one* **9**, e114669.
42. Li Y., Xu Y., Benitez B.A., Nagree M.S., Dearborn J.T., Jiang X.,... and Sands M.S. (2019) Genetic ablation of acid ceramidase in Krabbe disease confirms the psychosine hypothesis and identifies a new therapeutic target. *Proc Natl Acad Sci U S A* **116**, 20097-20103.
43. Jeon Y.J., Jung N., Park J.W., Park H.Y.and Jung S.C. (2015) Epithelial-Mesenchymal Transition in Kidney Tubular Epithelial Cells Induced by Globotriaosylsphingosine and Globotriaosylceramide. *PloS one* **10**, e0136442.
44. Rombach S.M., van den Bogaard B., de Groot E., Groener J.E., Poorthuis B.J., Linthorst G.E.,... and Aerts J.M. (2012) Vascular aspects of Fabry disease in relation to clinical manifestations and elevations in plasma globotriaosylsphingosine. *Hypertension* **60**, 998-1005.
45. Sanchez-Nino M.D., Sanz A.B., Carrasco S., Saleem M.A., Mathieson P.W., Valdivielso J.M.,... and Ortiz A. (2011) Globotriaosylsphingosine actions on human glomerular podocytes: implications for Fabry nephropathy. *Nephrol Dial Transplant* **26**, 1797-1802.
46. Realini N., Solorzano C., Pagliuca C., Pizzirani D., Armirotti A., Luciani R.,... and Piomelli D. (2013) Discovery of highly potent acid ceramidase inhibitors with in vitro tumor chemosensitizing activity. *Sci Rep* **3**, 1035.

47. Ouairy C.M., Ferraz M.J., Boot R.G., Baggelaar M.P., van der Stelt M., Appelman M.,... and Overkleeft H.S. (2015) Development of an acid ceramidase activity-based probe. *Chemical communications* **51**, 6161-6163.
48. Ordonez Y.F., Abad J.L., Aseeri M., Casas J., Garcia V., Casasampere M.,... and Fabrias G. (2019) Activity-Based Imaging of Acid Ceramidase in Living Cells. *Journal of the American Chemical Society* **141**, 7736-7742.
49. Rubboli G., Veggiotti P., Pini A., Berardinelli A., Cantalupo G., Bertini E.,... and Michelucci R. (2015) Spinal muscular atrophy associated with progressive myoclonic epilepsy: A rare condition caused by mutations in ASAH1. *Epilepsia* **56**, 692-698.
50. Marques A.R., Mirzaian M., Akiyama H., Wisse P., Ferraz M.J., Gaspar P.,... and Aerts J.M. (2016) Glucosylated cholesterol in mammalian cells and tissues: formation and degradation by multiple cellular beta-glucosidases. *J Lipid Res* **57**, 451-463.
51. Mirzaian M., Wisse P., Ferraz M.J., Marques A.R.A., Gaspar P., Oussoren S.V.,... and Aerts J.M. (2017) Simultaneous quantitation of sphingoid bases by UPLC-ESI-MS/MS with identical (13)C-encoded internal standards. *Clin Chim Acta* **466**, 178-184.
52. Schneider C.A., Rasband W.S.and Eliceiri K.W. (2012) NIH Image to ImageJ: 25 years of image analysis. *Nat Methods* **9**, 671-675.
53. Koch B.E., Stougaard J.and Spaink H.P. (2014) Spatial and temporal expression patterns of chitinase genes in developing zebrafish embryos. *Gene Expr Patterns* **14**, 69-77.
54. Nguyen-Chi M., Laplace-Builhe B., Travnickova J., Luz-Crawford P., Tejedor G., Lutfalla G.,... and Djouad F. (2017) TNF signaling and macrophages govern fin regeneration in zebrafish larvae. *Cell Death Dis* **8**, e2979.
55. Harjula S.E., Ojanen M.J.T., Taavitsainen S., Nykter M.and Ramet M. (2018) Interleukin 10 mutant zebrafish have an enhanced interferon gamma response and improved survival against a Mycobacterium marinum infection. *Sci Rep* **8**, 10360.
56. Tang R., Dodd A., Lai D., McNabb W.C.and Love D.R. (2007) Validation of zebrafish (Danio rerio) reference genes for quantitative real-time RT-PCR normalization. *Acta Biochim Biophys Sin (Shanghai)* **39**, 384-390.
57. Waterhouse A., Bertoni M., Bienert S., Studer G., Tauriello G., Gumienny R.,... and Schwede T. (2018) SWISS-MODEL: homology modelling of protein structures and complexes. *Nucleic acids research* **46**, W296-W303.
58. McNicholas S., Potterton E., Wilson K.S.and Noble M.E. (2011) Presenting your structures: the CCP4mg molecular-graphics software. *Acta Crystallogr D Biol Crystallogr* **67**, 386-394.